Turbulent flow over three-dimensional dunes: 1. Free surface and flow response

T. B. Maddux

Department of Applied Ocean Physics and Engineering, Woods Hole Oceanographic Institution, Woods Hole, Massachusetts, USA

J. M. Nelson

Water Resources Division, U.S. Geological Survey, Denver, Colorado, USA

S. R. McLean

Department of Mechanical and Environmental Engineering, University of California, Santa Barbara, California, USA

Received 6 January 2003; revised 13 June 2003; accepted 26 August 2003; published 11 December 2003.

[1] A series of detailed measurements were made of unidirectional turbulent open-channel flow over fixed, artificial, sinuous-crested three-dimensional (3-D) dune shapes. The response of the mean free surface was two-dimensional (2-D). Mean streamwise velocities were largest over the node of the sinuous dune crest line rather than over the maxima or minima of the crest line. Friction coefficients of the 3-D dunes were 50% higher on average in comparison to those of their 2-D counterparts when subjected to flows of similar depths and discharges. Despite the larger friction of the 3-D dunes, the turbulence generated by them was much weaker than that generated by their 2-D counterparts. The spatial structure of turbulence caused by the sinuous crest line of the 3-D dunes was correlated with the presence of secondary currents. These secondary current cells directed flow upward in the regions where the streamwise velocities were low and downward in the regions where streamwise velocities were high, suggesting that they could be responsible for a significant amount of momentum flux not being carried by the low turbulent stresses over the 3-D dunes. *INDEX TERMS:* 4219 Oceanography: General: Continental shelf processes; 4235 Oceanography: General: Estuarine processes; 4546 Oceanography: Physical: Nearshore processes; 4558 Oceanography: Physical: Sediment transport; 4568 Oceanography: Physical: Turbulence, diffusion, and mixing processes; *KEYWORDS:* dunes, ripples, turbulence, 3-D, free surface, Reynolds stress

Citation: Maddux, T. B., J. M. Nelson, and S. R. McLean, Turbulent flow over three-dimensional dunes: 1. Free surface and flow response, *J. Geophys. Res.*, *108*(F1), 6009, doi:10.1029/2003JF000017, 2003.

1. Introduction

[2] When exposed to a turbulent fluid flow, erodible beds that are initially flat often deform into wavy shapes or bed forms as a response to the fluid forcing. These bed forms have been observed in a wide variety of flows, including tidal estuaries and bays [*Dalrymple et al.*, 1978], on the continental shelf [*Flemming*, 1978; *Ardhuin et al.*, 2002], in rivers [*Sukhodolov et al.*, 1998; *Carling et al.*, 2000], and in the surf zone [*Gallagher et al.*, 1998; *Hanes et al.*, 2001]. For unidirectional subcritical flows of sufficient velocity, observed bed forms are classified as either ripples or dunes [*Simons and Richardson*, 1963; *Guy et al.*, 1966]. Because ripples have wavelengths much less than the flow depth, their effects are only exerted close to the bed, while they act on the flow far from the bed solely as increased bed roughness. On the other hand, dunes [*Ashley*, 1990] have longer wavelengths and produce topographic accelerations and decelerations of the flow field all the way to the free surface. Dunes in bed load-dominated and/or laboratory environments are often asymmetric, having low-sloping upstream side (stoss) sides and steep lee faces [*Yalin*, 1964; *Guy et al.*, 1966; *Kostaschuk*, 2000], while those in suspended-load-dominated environments are often more symmetric, with relatively low-angle lee faces [*Smith and McLean*, 1977; *Kostaschuk and Villard*, 1996; *Villard and Kostaschuk*, 1998; *Best and Kostaschuk*, 2002].

[3] The flow over an asymmetric dune separates at the crest, creating a large separation zone in the trough. Overlying or bounding the separation zone is a turbulent shear layer, and encompassing that shear layer is a turbulent wake that spreads and dissipates with distance downstream [*Raudkivi*, 1963; *McLean and Smith*, 1986]. The flow reattaches approximately 4–6 dune heights downstream of the crest [*Engel*, 1981]. Downstream of the point of reattachment, a new boundary layer develops and grows as flow accelerates toward the crest of the next dune. This flow structure results in high pressure downstream of the reattachment point on the stoss of the dune and low pressure on

0148-0227/03/2003JF000017$09.00

the steep lee face. The difference in pressure between the stoss and lee sides produces a net force on the dune called form drag. Above the wake and separation zone there is a quasi-inviscid interior region that is affected by mild spatial accelerations and the wakes of the upstream dunes [*Nelson and Smith*, 1989]. Although there is often not a persistent region of mean flow separation in flows over symmetric dunes, the flow deceleration in the lower lee results in the generation of an intermittent shear layer. This shear layer is capable of generating eddies and associated turbulence features which are analogous to those found over asymmetric dunes [*Best and Kostaschuk*, 2002].

[4] The general features of flow response to 2-D dune bathymetry are well understood. In order to understand in detail the specifics of the flow response to dunes, many researchers have studied fixed, artificial shapes in a laboratory setting. This allowed detailed studies of the flow without the added difficulty of measurement over a mobile bed. Previous laboratory experiments have been conducted over both asymmetric dunes [*Raudkivi*, 1963, 1966; *van Mierlo and de Ruiter*, 1988; *Lyn*, 1993; *Nelson et al.*, 1993; *McLean et al.*, 1994; *Bennett and Best*, 1995; *Cellino and Graf*, 2000; *Venditti and Bennett*, 2000] and symmetric features including high-angle and low-angle ripples [*Wiberg and Nelson*, 1992], low-angle dunes [*Best and Kostaschuk*, 2002], wavy pipes [*Hsu and Kennedy*, 1971], and wavy walls [*Hudson et al.*, 1996]. The remainder of this introduction will focus on asymmetric dunes, although it has been shown that many of the features to be discussed are present in flows over low-angle dunes due to intermittent flow separation [*Best and Kostaschuk*, 2002].

[5] Observations in the interior of relatively deep flows showed that the flow responds to dunes solely as roughness elements. For example, mean velocity defect profiles are semi-logarithmic [*Lyn*, 1993] in the interior. Also, in this region turbulence statistics observed in flows with Froude numbers that differed by a factor of three matched each other to within about 10% when scaled by u_*^T, the shear velocity associated with the total boundary shear stress [*McLean et al.*, 1994]. These observations of the interior flow were confirmed both in the field [*Sukhodolov et al.*, 1998] and for flow over a smooth rigid wavy boundary [*Hudson et al.*, 1996].

[6] Near the bed, the momentum defect associated with the separation zone is advected downstream as it diffuses. This results in a spatial acceleration that couples with a topographically induced acceleration due to the rising dune height downstream. This acceleration reduces the size of the separation zone relative to the size of the separation zone downstream of backward facing steps [*Engel*, 1981]. It has also been shown that the rate of decay of turbulent intensity downstream of dunes is much greater than that for flows downstream of a backward step or in typical 2-D wakes [*Nelson et al.*, 1993]. These accelerations affect the turbulence field and mean flow momentum balance in ways that could not be predicted using the total boundary shear stress [*McLean et al.*, 1994].

[7] Observations of turbulence have consistently found maxima in turbulent shear stresses, intensities, and production in the shear layer downstream of the dune crest. Turbulence generated by the shedding of eddies is downwardly advected by the mean flow toward the bed, causing it to interact with the newly developing boundary layer downstream of reattachment. As it is carried toward the next dune crest, wake turbulence decays and diffuses into the flow interior, and the largest stresses are found within the internal boundary layer. Turbulent correlation coefficients are [*Nelson et al.*, 1993] anomalously low, between 0.1 and 0.2 over the lower portions of the stoss sides of dunes, as compared with values from uniform boundary layers of 0.4 [*Hinze*, 1975; *Schlichting*, 1979]. These low coefficients arise due to the presence of uncorrelated wake turbulence interacting with the boundary layer [*McLean et al.*, 1994] and increase toward a value of 0.4 at the dune crest. In addition, the near-bed Reynolds shear stresses differ from estimates based on of the shear of mean velocity profiles in the same regions of the trough, with correlation improving toward the crest [*McLean et al.*, 1996]. Anomalous turbulent stresses such as these were also reported by early investigations of turbulent flow over dunes [*Raudkivi*, 1966].

[8] The structure of mean flow and turbulence near the bed violates the assumptions typically used to create sediment transport relations for uniform flows. In particular, this implies that the near-bed Reynolds shear stresses could be used neither to estimate the mean rate of sediment transport over dunes nor to estimate their growth and morphological evolution [*Nelson et al.*, 1995]. Therefore attempts to predict the details of the transport of sediment over dunes are often inaccurate.

[9] The vast majority of laboratory research to date has been focused on the study of 2-D dunes; indeed no detailed experiments have been conducted over 3-D dunes. Natural dunes are often three-dimensional. They can exhibit cross-stream variations in crest height or in the streamwise crest location [*Allen*, 1982], with phase differences between successive crest lines leading to variations in dune wavelength and steepness [*Gabel*, 1993]. Natural 3-D dunes can take on very complex shapes, such as those of barchan dunes [*Embabi and Ashour*, 1993], or lunate dunes [*Allen*, 1982], which are dissimilar from the 2-D features typically studied in laboratory experiments. An additional feature of many 3-D dunes is the presence of scour pits in the dune troughs. Three-dimensional dune fields observed with these pits are irregular and the underlying physics leading to the pit locations is not understood [*Dalrymple et al.*, 1978; *Costello and Southard*, 1981].

[10] Because of the importance of dunes in controlling sediment transport rates, generating turbulence, and creating flow resistance, it is essential that a detailed understanding be acquired of flow response to more natural 3-D dune shapes than have been studied in the laboratory. The objective of the present study is to extend the understanding acquired from measurements over asymmetric 2-D dunes by conducting similarly well-controlled experiments over a set of asymmetric 3-D dunes. These fixed, artificial, asymmetric 3-D dunes, though simple in some respects, incorporate many observed features of natural dunes while maintaining enough similarity on average to previously studied asymmetric 2-D dunes to allow detailed comparisons. The dunes were constructed to allow the flow to route itself around bathymetric highs but do not possess scour pits. This allowed unambiguous comparisons of the observations over 3-D dunes with previous observations over 2-D dunes.

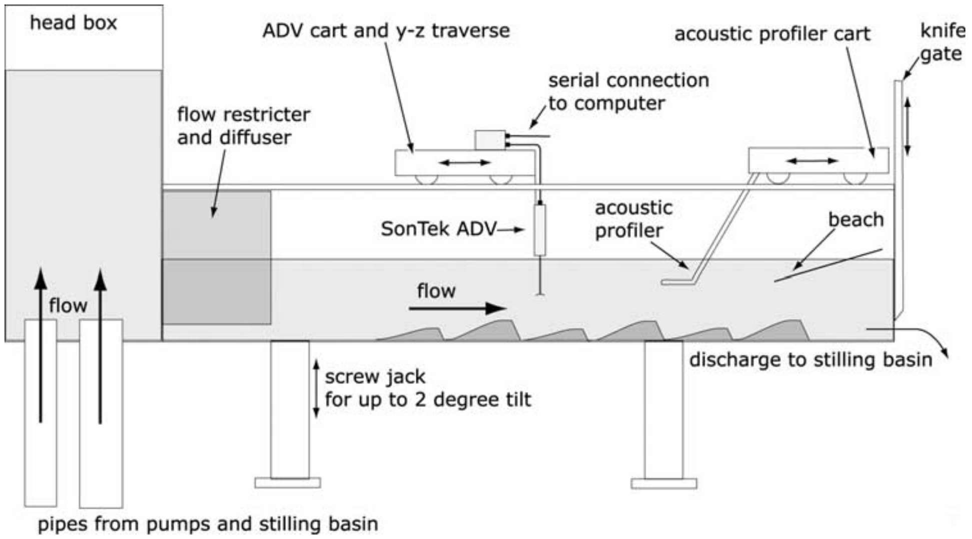

Figure 1. Side view illustration of the tilting-recirculating flume, with associated equipment and artificial bed forms used in these experiments. Not shown are the pumps and large stilling basin.

[11] The results of the study are presented in this paper and the companion paper by *Maddux et al.* [2003]. In this paper, laboratory observations of turbulent open-channel flow over the fixed, artificial, asymmetric 3-D dunes are presented. A vertically averaged (hydrostatic) model will be shown to underpredict the steering of the flow around high points of 3-D dune crests. It will be shown that this observed steering produces different turbulent and mean flow structures than were previously observed over 2-D dunes. In particular, the 3-D dunes exert more friction on the flow than 2-D dunes while generating less turbulence. This is hypothetically due to the presence of secondary currents that were correlated with the cross-stream structures of mean flow and turbulence. In the second paper, this hypothesis is tested using a spatial averaging technique, and various estimates of the total boundary shear stress are compared. In particular, it will be confirmed by *Maddux et al.* [2003] that the spatially averaged Reynolds shear stress alone cannot be used to predict the total boundary shear stress over the 3-D dunes, unlike the 2-D dunes.

2. Experimental Procedure

2.1. Facilities and Equipment

[12] All of the experiments were conducted in the tilting-recirculating flume (Figure 1) in the Ocean Engineering Lab (OEL) at the University of California, Santa Barbara. The flume is 22 m in length, with a 0.9 m × 0.9 m cross section, and is tiltable to 2°. Two pumps deliver a discharge of up to 0.35 m^3/s [*McLean et al.*, 1994] through four pipes (two from each pump) vertically into the head box. The water exits the head box through a wooden flow restrictor and then enters the flume. The walls of the flume are glass, and the bottom is steel covered with a thin layer of concrete to make it even. A downward closing knife gate at the end of the flume controls the water depth. Water flowing past the gate falls into a large stilling basin. To ensure the same operating conditions from experiment to experiment, all water depths and the pump discharge are monitored. Surface waves are damped at both ends of the flume. The coordinate system of the measurements is as follows: x positive downstream, z positive upward, and y positive in the cross-stream direction such that it defines a right-hand coordinate system (90° to the left of the x axis when viewed from above). Steps were taken to ensure that the flow in the flume was two-dimensional away from the walls when operating with a flat bottom [*Maddux*, 2002].

[13] Fourteen fixed artificial 3-D dunes were fabricated and placed in the flume (Figure 2). The dunes were fashioned from a wooden frame and covered with thin (~1/16 inch) lead sheets on the upstream side and acrylic plastic on the downstream side. The dunes were painted and roughened with coarse sand (diameter 1 mm) that was sprinkled atop the wet paint. Joints between adjacent dunes were sealed with waterproof caulking, and each dune spanned almost the entire width of the flume, with the remaining gap between dune and glass wall being sealed with foam pipe insulation. Single 1–2 mm diameter holes were drilled into the high crest of each dune to allow air to escape when starting an experiment.

[14] The dunes had a mean wavelength $\langle\lambda\rangle$ of 0.8 m and a mean height $\langle H\rangle$ at the crest of 0.04 m. The stoss side of the dunes was a half-cosine wave running from its low point at the trough to its high point at the crest. The angle of the lee slope was 30°. The mean height, wavelength, steepness, and cross section of these dunes matched those of 2-D dunes used in experiments conducted at the OEL [*McLean et al.*, 1994] and other locations [*Nelson and Smith*, 1989; *Nelson et al.*, 1993]. This was done to allow meaningful comparisons of the data collected during the experiments with previous results.

[15] The three dimensionality of the dunes was expressed as a full cosine wave in the cross-stream direction, superimposed on the profile of the 2-D dunes. The height of the crests of the dunes above the troughs, H, varied in the cross-stream direction from 0.02 to 0.06 m. Successive crest lines were 180° out of phase, so that a dune with a high middle and low sides was followed immediately by a dune with a low middle and high sides, as shown in Figure 2. This is consistent with observations of sinuous-crested and barchan

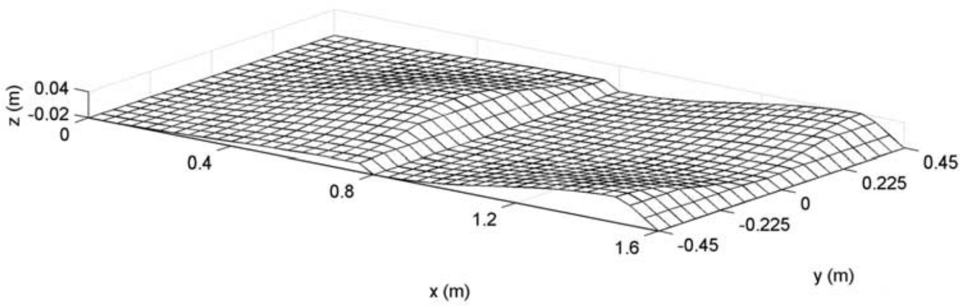

Figure 2. Schematic of the 3-D fixed, artificial dunes used in the experiments. Flow over the dunes runs from top left to bottom right.

dunes [*Shehata et al.*, 1992; *Embabi and Ashour*, 1993]. It resulted in a crest-to-crest wavelength, λ, that varied in the cross-stream direction from 0.73 to 0.87 m. The resulting steepness of the dunes varied in the cross-stream direction as well, with H/λ values ranging from 0.02 to 0.08. These values are consistent with values of H/λ for real dunes in the field [*Ashley*, 1990; *Gabel*, 1993; *Julien and Klaassen*, 1995]. The artificial 3-D dunes were qualitatively similar to real sinuous-crested asymmetric 3-D dunes as observed in the field and in flumes with mobile sediments [*Ashley*, 1990; *Gabel*, 1993; *Julien and Klaassen*, 1995]. Although typical 3-D dunes are often more complex, with concave faces and other features, these dunes are sufficiently realistic while maintaining enough similarity to previous measurements to facilitate an understanding of the response of the flow to 3-D bed topography.

[16] A 5 MHz up-down looking acoustic profiler with a 0.3 mm vertical resolution was used both for measurements of the mean free surface as well as to check for spatial and temporal equilibrium of the flume. The profiler was mounted on a tow carriage and run repeatedly along the test section during operation to ensure that the mean slope of the free surface matched the mean slope of the bottom. Differences in this slope were resolvable to within ±0.00003 [*McLean et al.*, 1994]. Once the mean bottom slope and mean free surface slope matched, the tilt of the flume was measured using a micrometer. The total boundary shear stress was estimated from this measurement (see *Maddux et al.* [2003] for results of this and other estimates).

[17] A 10 MHz 5 cm SonTek acoustic Doppler velocimeter (ADV) [*Kraus et al.*, 1994; *SonTek*, 1995] is also mounted atop the tilting-recirculating flume. Both a three-axis downward looking and a two-axis side-looking probe were used; the two-axis probe was used for making measurements near the free surface. The ADV samples turbulent velocity values at a rate of up to 25 Hz in a small sampling volume ~5 cm distant from the probe tip. Using a technique known as pulse-to-pulse coherent Doppler sonar [*Lhermitte and Serafin*, 1984], the phase shift between successive backscattered signals sampled at each receiver is converted to a measurement of velocity along each beam. Factory calibration of the ADV permits conversion of the along-beam velocities into an orthogonal coordinate system. Errors in the prediction of mean velocities are no greater than ±2.5 mm/s ±1% [*Kraus et al.*, 1994; *SonTek*, 1995; *Snyder and Castro*, 1999]. The ADV has been validated through comparisons with several other devices (for a review, see *Maddux* [2002]) and has been used in a variety of applications to measure turbulent flows, such as over 2-D dunes [*Venditti and Bennett*, 2000] and in the surf zone [*Elgar et al.*, 2001; *Trowbridge and Elgar*, 2001].

[18] Each of the received signals along each channel or receiver beam carries noise, which has the potential to bias measured values of turbulent quantities. The noise along each beam is uncorrelated with and of equal magnitude to the noise along the other beams. It is unbiased (zero mean) and does not affect mean velocity measurements, if data is acquired for a sufficient time [*Lohrmann et al.*, 1995]. The noise is white [*Lohrmann et al.*, 1994] and uncorrelated with the actual velocity fluctuations [*Voulgaris and Trowbridge*, 1998]. Because of these features and the geometry of the ADV probe, the noise results in negligible bias of measured Reynolds shear stresses, slight bias of measured vertical velocity variances, and significant noise bias in measured horizontal velocity variances [*Lohrmann et al.*, 1995; *Maddux*, 2002].

[19] Noise bias may be reduced through careful selection of the maximum velocity range of the ADV or estimated from the "noise floor" visible in velocity power spectra at high frequencies. Since the total noise variance is due to pure white noise, the noise floor at high frequencies can be extrapolated across all measured frequencies and then integrated to obtain an estimate of the noise. This procedure has been confirmed by measurements of uniform open-channel flows [*Nikora and Goring*, 1998; *Voulgaris and Trowbridge*, 1998]. It was also tested using measurements of separated and unseparated flows (data not shown) over the 3-D dunes and was subsequently used in the current study.

2.2. Study of Flow and Free Surface Over the 3-D Dunes

[20] Experiments were conducted over the 3-D dunes for flow of similar depth and discharge as for runs 2 and 3 [*McLean et al.*, 1994] over the 2-D dunes (Table 1). Both detailed velocity measurements using the ADV and mappings of free surface topography using the acoustic profiler were performed. All measurements were conducted over the eleventh and twelfth numbered dunes, with numbering starting at the most upstream dune, of the series of fourteen 3-D dunes. Two flow conditions (runs) for the flume were set for the experiments, named runs T2 and T3. The flume tilt (and hence mean free surface slope S) was measured with a micrometer at the start of each run.

Table 1. Experimental Conditions for Runs T2 and T3 as Well as Runs 2 and 3 Over the 2-D Dunes[a]

Run	h_0, m	U, m/s	Fr	τ_T, Pa	u_*^T, m/s	C_f	S, $\times 10^4$
T2	0.173	0.357	0.275	1.71	0.0413	0.0134	10.6
T3	0.561	0.261	0.111	0.46	0.0215	0.0068	2.40
2	0.158	0.377	0.303	1.07	0.0327	0.0075	9.4
3	0.546	0.284	0.123	0.40	0.0200	0.0050	0.81

[a]From *McLean et al.* [1994, 1999].

[21] Direct measurements of velocity were made using the ADV in vertical profiles at a wide variety of locations throughout the flow field. These locations are denoted by the dots in Figure 3. Vertical profiles were spaced every 0.04 m in the x direction, which matched the measurement spacing over the 2-D dunes. Profiles were also spaced every 0.045 m in the y direction. Data was collected from the bed to the free surface and from the centerline of the flume ($y = y_2 = 0$ m) to the halfway point between the centerline and the wall ($y = y_1 = -0.225$ m), over two wavelengths of individual dunes (from $x = x_1 = 0$ m to $x = x_2 = 1.6$ m). This was done for several reasons. First, the goal of the experiment was to measure the flow as if it were in a very wide field of dunes, with no sidewalls present. Venturing closer to the walls of the flume was not done, therefore, so that the presence of the walls would not affect the measurements. Second, if the experiment were perfectly set up, the flow would be symmetric about the centerline, and measurements in the other half of the flume (from the centerline to the other wall) would be redundant. Checks were performed to test whether the flow field was symmetric, and although it was not perfect, measured asymmetries were judged to be insignificant [*Maddux*, 2002]. However, as indicated by *Maddux et al.* [2003], these seemingly small departures from symmetry give rise to significant momentum fluxes. Finally, it would have taken four times as long to measure the entire flow field.

[22] The vertical spacing of individual data points within each profile was approximately logarithmic relative to the local bed elevation, starting from a few millimeters off the bed, for a total of between 20 and 30 data points, depending on the local flow depth. Velocity measurements were collected using the three-axis probe except for measurement points during run T2 that were too close to the free surface to allow the three-axis probe to be used. The two-axis probe was used to measure this uppermost portion of the water column. During run T3, no measurements were taken using the two-axis probe.

[23] Before the start of each vertical profile, the water temperature was measured to within ±0.1°C, to prevent errors associated with poor estimation of the speed of sound. The ADV was then used to establish its location relative to the local bed elevation. With the 3-D probe, a series of 30 acoustic pulses were emitted by the ADV and averaged to estimate the distance of the sampling volume from the bed. This procedure was accurate to within ±0.2 mm, assuming the ±1 mm measurement error of a single pulse [*SonTek*, 1995] is normally distributed. With the 2-D probe, the ADV was moved downward until it was observed to be touching the bed. Subsequent elevations of the ADV were tracked with optical encoders. The encoders resolve the ADV location to within ±0.2 mm in x, ±0.5 mm in y, and ±0.05 mm in z.

[24] At each vertical location, the maximum velocity range setting of the ADV was set to as low a value as possible, depending on the flow conditions being measured. The bottom was pinged once more to adjust for pulse-boundary interference, and then data was collected by the ADV for 120 s at a rate of 25 Hz, totaling 3000 time series data points. Afterward, data points with ADV beam correlations <70% were replaced by mean values and the time series was recorded. The contributions of noise to measured velocity variances were next estimated using the high-frequency "tails" of power spectra and subtracted from the measured velocity variances. Finally, the corrected variances were recorded along with vectors of mean velocity, Reynolds shear stress, skewness, and kurtosis.

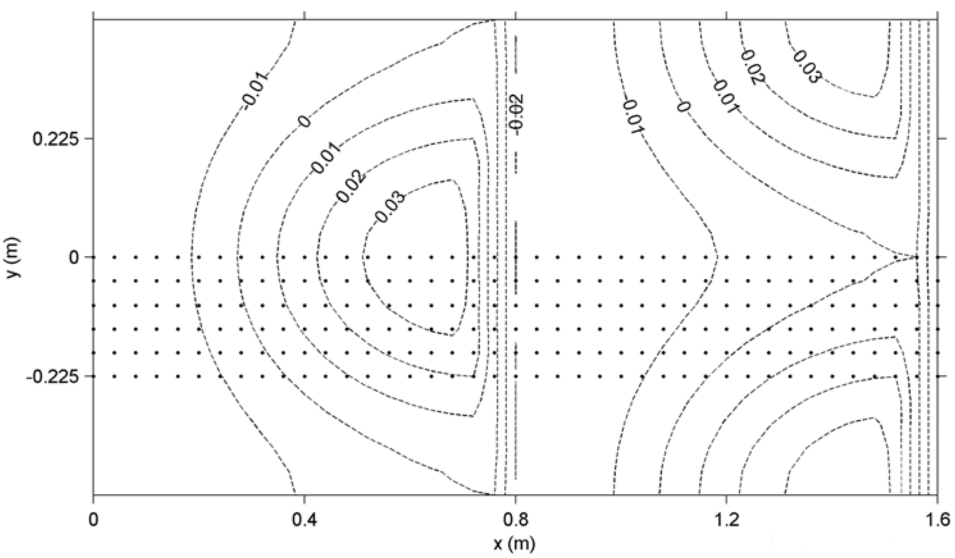

Figure 3. Bed elevation (η) of the 3-D dunes (dashed contour lines and associated labels) in meters, with the locations of vertical velocity profiles and mean free surface measurement points illustrated (dots).

[25] Data collected by the two probes were combined [*Maddux*, 2002] to form a single data set for run T2. Since the 2-D probe did not measure any vertical velocities, estimates of vertical velocity were obtained from the continuity equation:

$$\bar{w} = -\int \left(\frac{\partial \bar{u}}{\partial x} + \frac{\partial \bar{v}}{\partial y} \right) dz, \tag{1}$$

where w is the vertical velocity, u is the downstream velocity, v is the cross-stream velocity, and overbars denote time averaging. The integral was performed upward from the last point in the velocity profile for which measurements were made with the 3-D probe. Linear interpolations of the components of the Reynolds stress tensor containing vertical velocity fluctuations, denoted by $\overline{u'w'}$, $\overline{v'w'}$, and $\overline{w'^2}$ where primes denote a time-fluctuating quantity, were made between their value at that last point and a value of zero at the free surface. The final step applied to data sets from both runs was vertical smoothing with a three-point boxcar filter.

[26] The acoustic profiler was used to measure the topography of the time-averaged free surface over individual fixed dunes. Free surface measurements were made only for run T2, as previous work over 2-D dunes observed negligible free surface response for run 3 conditions. The profiler was operated in both the x direction at a series of cross-stream locations, and in the y direction at a series of streamwise locations throughout the flume. This yielded a series of 2-D slices or profiles of the overall 3-D free surface response. The 2-D profiles were digitally filtered, smoothed, down sampled to the grid of velocity measurements, and merged [*Maddux*, 2002] to yield a measurement of the mean (time-averaged) free surface topography (ζ) at every location where vertical velocity profiles were measured (Figure 3, dots).

3. Results and Discussion

3.1. Flow Conditions and Macroscopic Parameters

[27] The general flow conditions associated with the two runs over the 3-D dunes as well as their 2-D counterparts are shown in Table 1. Shown are the mean flow depth h_0, average velocity

$$U = \int_{x_1}^{x_2} \int_{y_1}^{y_2} \frac{1}{h_0 + \zeta - \eta} \int_{\eta}^{h_0+\zeta} \bar{u} dz dy dx,$$

where η denotes the local bed elevation, Froude number $Fr = U/\sqrt{gh_0}$, total boundary shear stress τ_T found from a linear fit to the results of the spatially averaged streamwise momentum (see *Maddux et al.* [2003] and *McLean et al.* [1999] for the 2-D dunes equation), its associated shear velocity $u_*^T = \sqrt{\tau_T/\rho}$, friction coefficient $C_f = \tau_T/\rho U^2 = (u_*^T/U)^2$, and mean free surface slope S.

[28] The initial goal was to maintain the same water depth and average velocity over the 3-D dunes as for previous experiments over 2-D dunes. However, the mean flow depth was accidentally set 1.5 cm too deep for runs T2 and T3, while the pumps delivered the same discharge to within ±6%. This resulted in a 5–8% reduction in average velocity and a 10% reduction in Froude number for runs T2 and T3 relative to runs 2 and 3. To compensate for this, the friction coefficients were calculated. Friction coefficients for the 3-D runs averaged 50% larger than those for the 2-D runs. At first glance, this is surprising given that the flow can conserve momentum by steering around the obstacle presented by a 3-D dune. However, flow steering near the bed also results in higher spatial variability in near-bed velocities, and areas of higher near-bed velocities contribute in a nonlinear fashion to the skin friction and form drag. Thus the additional spatial variability in the near-bed flow could result in higher total boundary shear stress.

3.2. The Free Surface

[29] Plots of mean free surface topography measurements and modeling are shown in Figures 4 and 5. Actual measurements were taken over the length of two individual dunes and over one-quarter width of the flume; the results from the measurement region have been transposed so that they cover the entire width of the flume. This assumes that the flow is symmetric about the flume centerline and that no walls are present, effectively making the flume infinitely long and wide. This was done only for the purpose of ease of visualization. These plots should not be taken as a representation of the actual flow field across the entire flume width, which remains largely unmeasured. *Maddux et al.* [2003] show that asymmetries in the mean flow and turbulence fields must be accounted for to close the momentum balance over the 3-D dunes. These asymmetries are small, of the order of the nominal accuracy of the ADV (±2.5 mm/s ±1%), and the general features of the flow field illustrated in this paper have been confirmed with selected cross-stream profiles of the flume width over both dunes (data not shown).

[30] Figure 4 shows the mean free surface measured during run T2 along with the results of a 2-D depth-averaged shallow water model. The measured free surface response was two-dimensional, with slight cross-stream variation and most of the response being that of a typical low Froude number flow over 2-D dunes, with the deeper water over the trough and shallow water over the crest. The amplitude of the free surface modulation was 1 mm. The relatively small cross-stream variation in the free surface topography suggests that the flow is topographically steered by the 3-D features. If the flow were not steered around the bed forms, one would expect a much greater free surface response over the highest and lowest features, resulting in more cross-stream variation of the free surface, as is seen in the bottom panel of Figure 4.

[31] These predictions of the mean free surface topography were made using a vertically integrated model of the shallow water equations of motion [*Nelson et al.*, 2003]. The model was run for the same average flow depth h_0 and mean flow rate U as observed during run T2. It predicted a much more 3-D free surface response, with low free surface elevations over the higher parts of the crest, and the amplitude of the modeled free surface response was twice that of the measured response. The model also made corresponding predictions of the depth-averaged velocity field, with weaker cross-stream flow and less steering [*Maddux*, 2002]. This shows that the steering of the flow is consistent with nonhydrostatic conditions, with most of the steering of the flow around the obstacles occurring near the bed and not in the interior, and

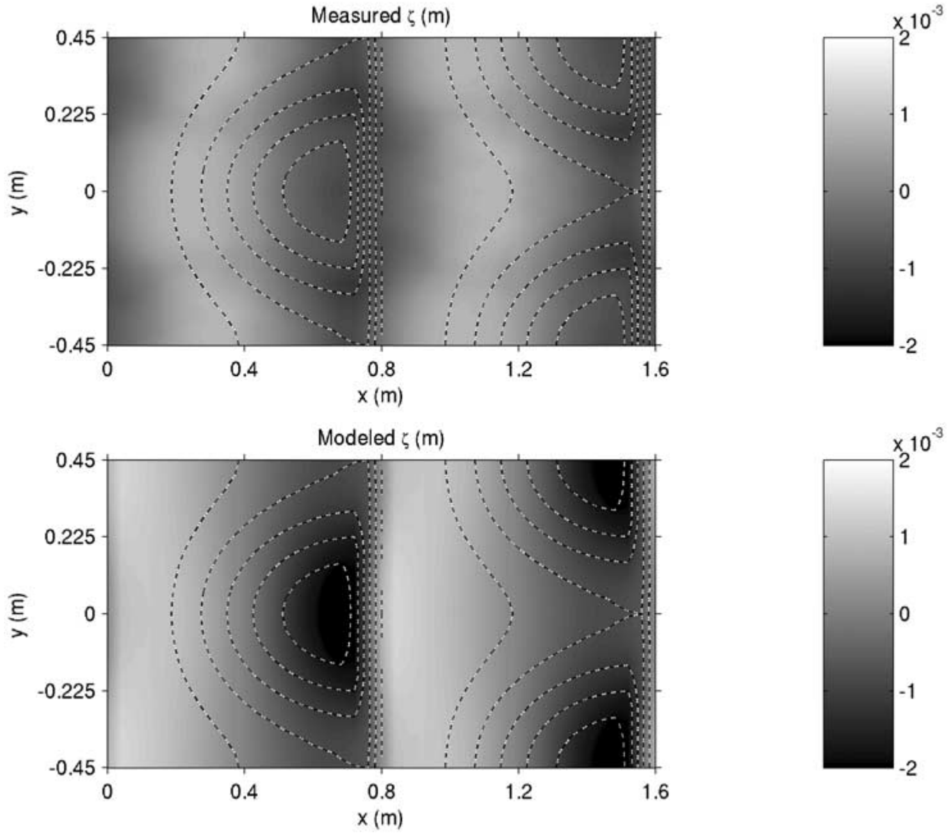

Figure 4. Mean free surface topography (ζ, shading) from (top) measurements and (bottom) 2-D shallow water model for run T2. Unlabeled bed elevation contours (η) are denoted by dashed lines in this and subsequent *x*-*y* figures. See color version of this figure in the HTML.

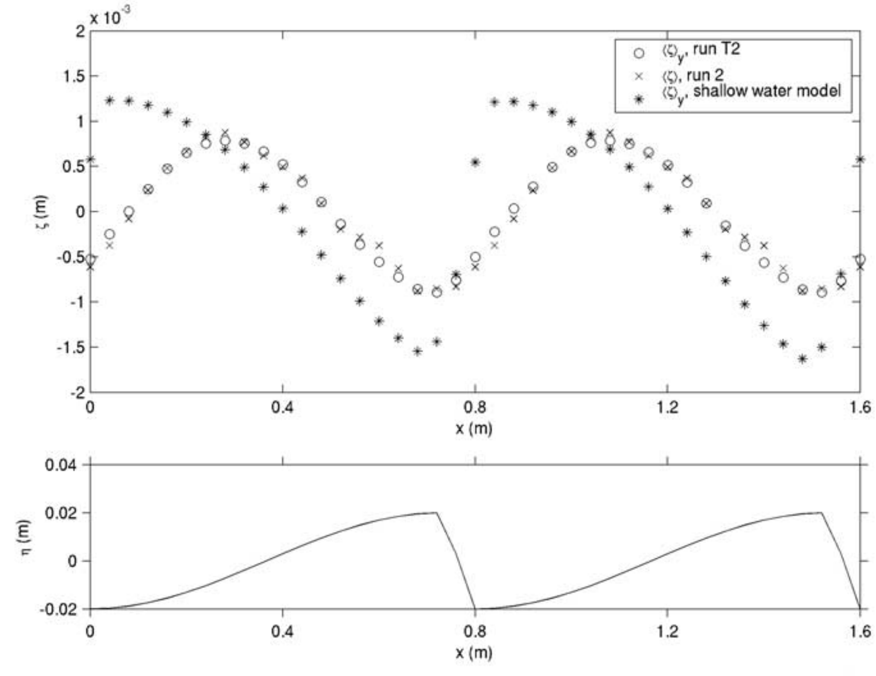

Figure 5. Cross-stream averages of (top) free surface topography measurements and models (symbols as noted) and (bottom) bottom bathymetry.

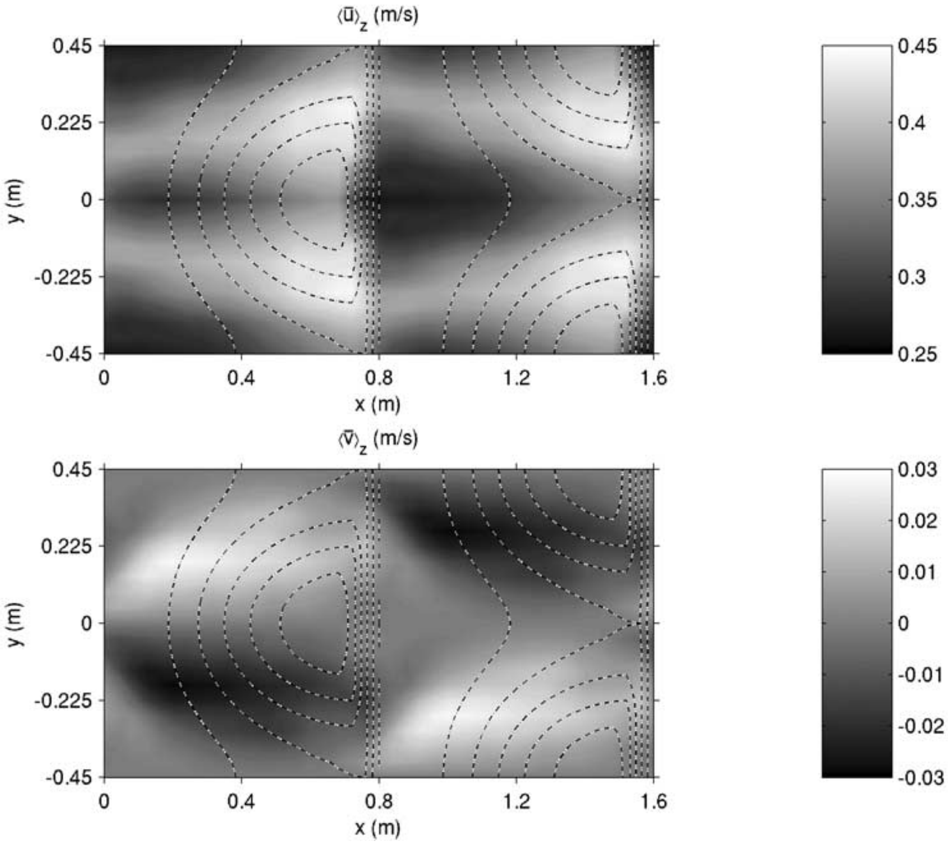

Figure 6. Depth-averaged (top) streamwise and (bottom) cross-stream velocities for run T2. See color version of this figure in the HTML.

thus the gross routing of the flow is incorrectly predicted with a vertically averaged model.

[32] The free surface measurements and model results were averaged in the cross stream and presented in Figure 5. Also shown for comparison is the measured free surface from run 2, which matched the cross-stream average of the measured free surface from run T2. The predicted amplitude of the average free surface was 50% greater than the measured average free surface. The predicted free surface was also in-phase with the dune bathymetry. Both of these prediction errors are consistent with the nonhydrostatic responses of the near-bed fluid to flow separation and its associated turbulence.

3.3. Depth-Averaged Flow Field

[33] A presentation of the mean values and turbulent statistics for all three components of velocity at all measurement locations would be intractable. To avoid this, contour plots of a subset of all the measurement results will be shown either for selected locations or for spatially integrated quantities. The streamwise, cross-stream, and depth averages of a flow variable are defined as

$$\langle F \rangle_x = \frac{1}{L_f} \int_{L_f} F(x', y, z, t) dx', \tag{2}$$

$$\langle F \rangle_y = \frac{1}{W_f} \int_{W_f} F(x, y', z, t) dy', \tag{3}$$

$$\langle F \rangle_z = \frac{1}{h_0 - \eta + \zeta} \int_{\eta}^{h_0+\zeta} F(x, y, z', t) dz', \tag{4}$$

respectively, where F is the flow quantity, angle brackets denote an averaged value, the subscript denotes the axis along which the average was taken, and finally L_f or W_f are the fluid-occupied portions of the length or width along which averaging was done, for an x average or a y average respectively. (Additional plots and animations that include visualizations of mean flow fields, velocity variances, turbulent kinetic energy, Reynolds shear stresses, cross-correlation coefficients, and shear production are available at http://www.me.ucsb.edu/3dunes/.)

[34] The depth-averaged mean velocities measured during run T2 are shown in Figure 6. The greatest streamwise velocities were not at the maxima of the dune crest line, but were at the node of the dune crest line, which was halfway between the highest and lowest parts of the crest. Cross-stream variability in streamwise velocity along the crest line was nearly 15% of the mean streamwise velocity at the crest line. Furthermore, the streamwise velocities at the highest and lowest parts of the crest line were nearly the same. These mean flow structures were confirmed with several cross-stream profiles of the entire flume width over both dunes (data not shown). Also apparent were a large wake behind the highest crest and another region of slower fluid behind the lowest crest.

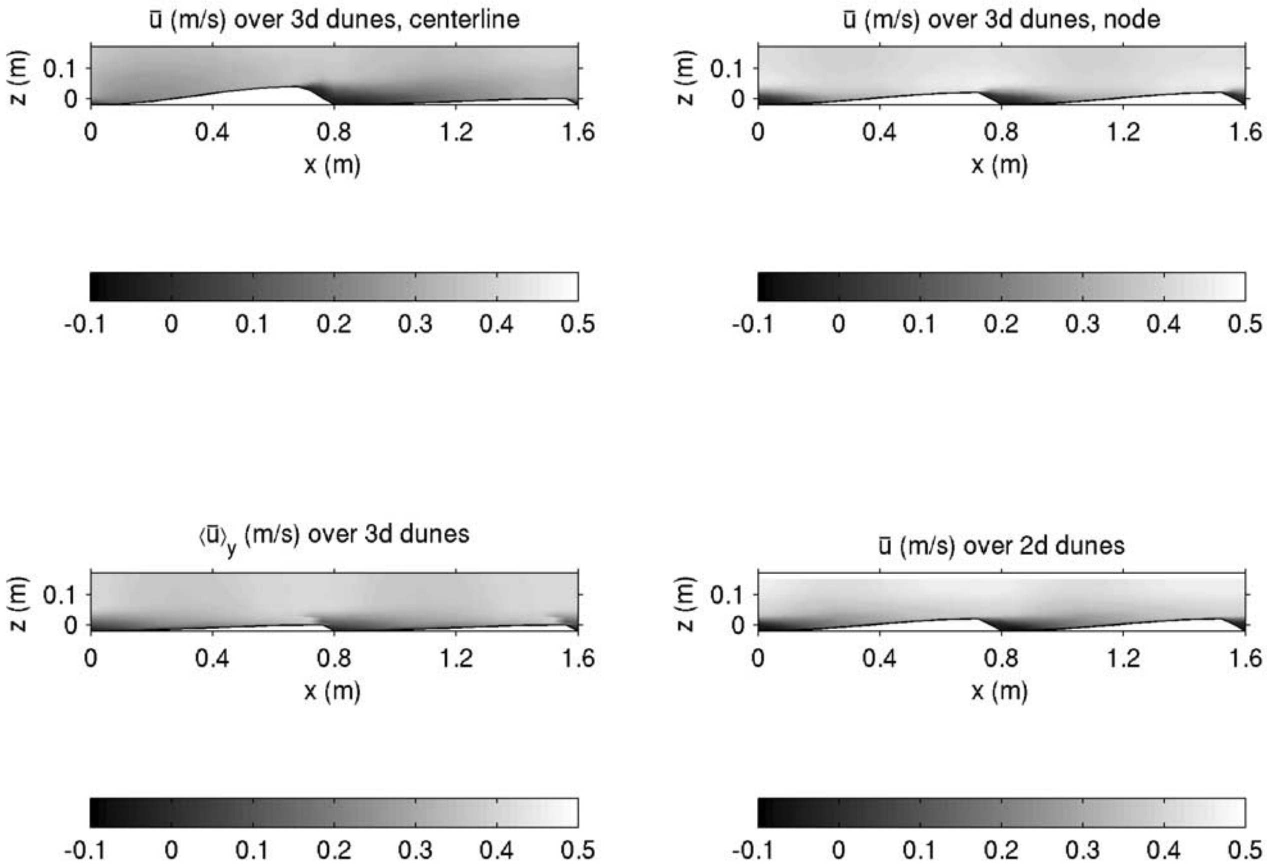

Figure 7. (top) Mean streamwise velocities for run T2 at two cross-stream locations: the centerline ($y = 0$ m) and the node ($y = -0.225$ m), or halfway between the centerline and the flume wall. Also shown are the cross-stream average of (bottom left) the streamwise velocity for run T2 and (bottom right) the streamwise velocity measured during run 2. See color version of this figure in the HTML.

[35] The largest cross-stream velocities were also in line with the node of the dune crest line. Most of the cross-stream flow started in the trough and near the bed. The flow was oriented to divert fluid around the top of the next dune downstream, as can be seen more clearly in animations of the mean cross-stream flow provided in the electronic supplement. Results for run T3 (data not shown) were similar, with the greatest streamwise flow over the crest line nodes and the greatest cross-stream flow in the trough downstream of the crest line nodes. The depth-averaged flow for run T3 had diminished horizontal variability due to greater flow depth.

3.4. Cross-Stream-Averaged Flow Field and 2-D Comparison

[36] Results of cross-stream averaging (equation (3)) applied to mean flow and turbulence parameters are presented in this section. They are compared with results from two cross-stream locations ($y = 0$ m, the flume centerline, and $y = -0.225$ m, the node of the dune crest line or halfway between the centerline and the flume wall). Also presented for comparison are results from previous measurements over 2-D dunes (runs 2 and 3, reported by *McLean et al.* [1994]).

[37] Streamwise mean velocity measurements from run T2 are shown in Figure 7. A large wake of slow fluid formed behind the high crest (upper left) because of flow separation; it extended nearly to the following low crest. A second region of very weak flow formed beyond the small crest as the flow moved back up to the high crest. This was previously noted in the depth-averaged flow discussion (Figure 6). This decelerated flow is neither associated with separation over the smaller crest just upstream nor the previous higher crest. It is more likely due to not only an increase in the cross-sectional area of the flow but also steering of the flow away from the high crest downstream. The greatest velocities were measured over the node of the crest line (upper right), halfway between the flume centerline and the wall. Flow rates over the node of the crest line were similar to those over the 2-D dunes (lower right), although the near-bed velocities were stronger over the 3-D dunes at about midway up the stoss side. The cross-stream average (lower left) was similar to both, but more comparable to the 2-D dunes as the wake region did extend farther downstream. The reduced backflow strength in the separation zone was likely due to the varying distribution of the separation point along the crest line of the 3-D dunes and due to the fact that streamwise velocities are relatively low over the maxima of the crest line.

[38] Results obtained during run T3 were similar, as shown in Figure 8. The streamwise flow over the highest

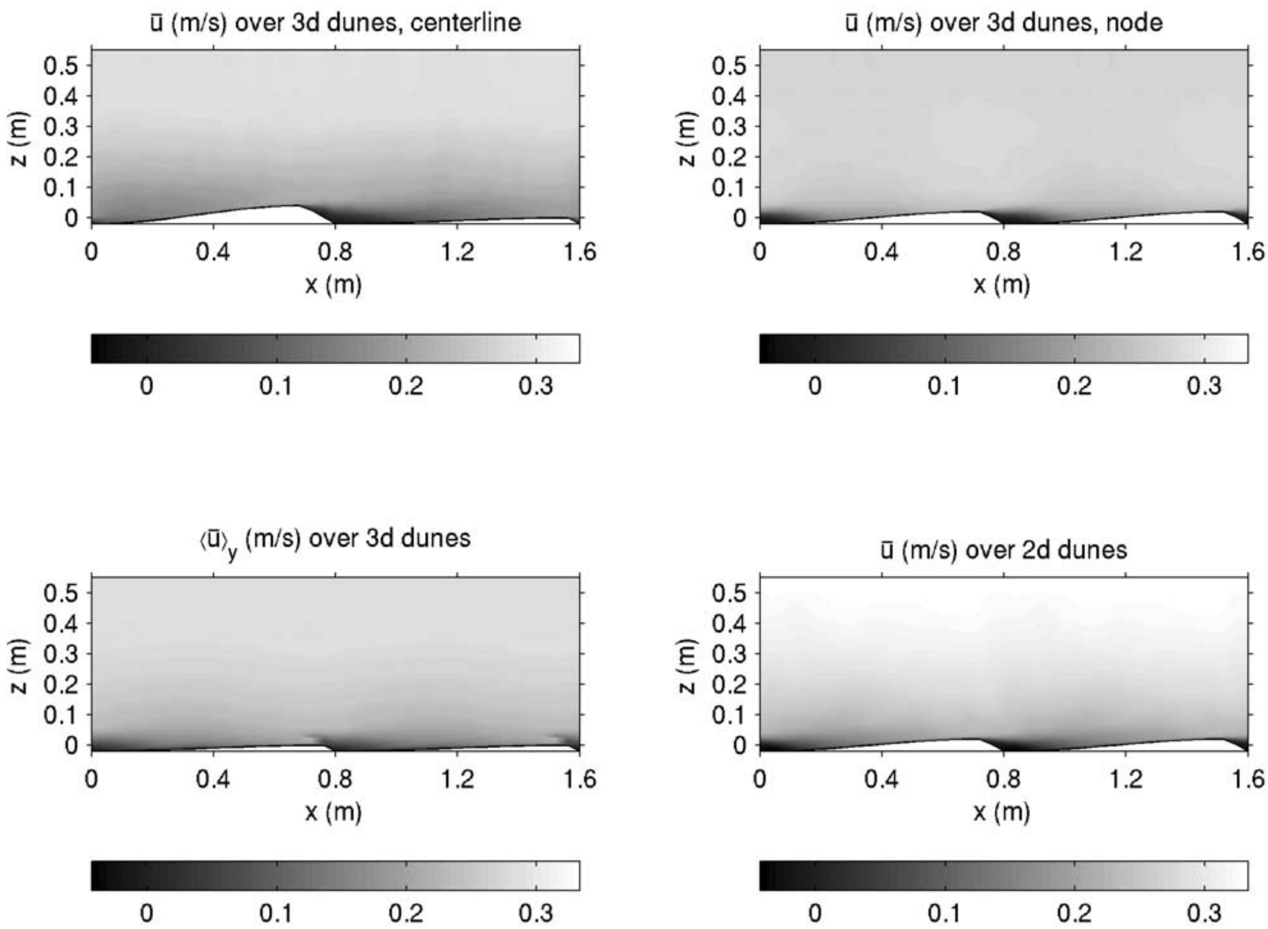

Figure 8. Mean streamwise velocities for run T3 at (top left) the centerline and (top right) the node. Also shown are the cross-stream average of (bottom left) the streamwise velocity for run T3 and (bottom right) the streamwise velocity measured during run 3. See color version of this figure in the HTML.

crest was again significantly slowed. This was not due to separation over the smaller crest just upstream, as its separation zone was so small that it was nearly unmeasured. Meanwhile, the acceleration of fluid flow up the stoss side toward the node of the crest was stronger than in any of the other contour plots: high crest, low crest, or even the 2-D dunes. Finally, with a larger flow interior than was present during run T2, the velocity field over the 3-D dunes was found to be relatively free of shear when compared to the 2-D dunes.

[39] Mean vertical velocities measured during run T2 are shown in Figure 9. Flow was directed up over the stoss side of the dunes and downward past the crest into the trough at all cross-stream locations. Some upward flow was also present near the lee of the dunes, illustrating the presence of a recirculating mean flow in the separation zone. These general features at different cross-stream locations deviated from the average behavior. The greatest upward velocities occurred upstream of the highest crest, and this was also the largest area of upward directed flow. This very strong upward flow, coupled with the diversion of fluid around the highest crest shown previously in Figure 6, was likely responsible for the slower streamwise flow over the high crest. Vertical flows associated with the low crest were weak but positive. The strongest downward velocities occurred downstream of the crest line node, and not downstream of the high crest. It was also there that the area of downward directed flow was largest. Overall, the vertical flow field at the node cross section was quite different from its counterpart over the 2-D dunes and biased negative by comparison. The cross-stream average of the mean vertical velocity was similar in magnitude to the vertical velocity field over the 2-D dunes.

[40] The corresponding vertical velocity fields for run T3 are shown in Figure 10. The structure was similar to the shallower flow case, with very different vertical flow response over different cross sections of the dune field. Absolute values of vertical velocity were 40% smaller for run T3 than for run T2. At all cross sections, the mean vertical velocities became quite small in the upper 0.3 m of the water column. The vertical response for run 3 was smaller and more diffuse relative to the average run T3 response. Vertical velocities over the stoss sides of the 2-D dunes were most favorably comparable to the vertical velocities running up to the lowest crest of the 3-D dunes.

[41] Observations of one component, $-\overline{u'w'}$, of the Reynolds shear stresses measured during run T2 are shown in Figure 11. The results were qualitatively similar to previous

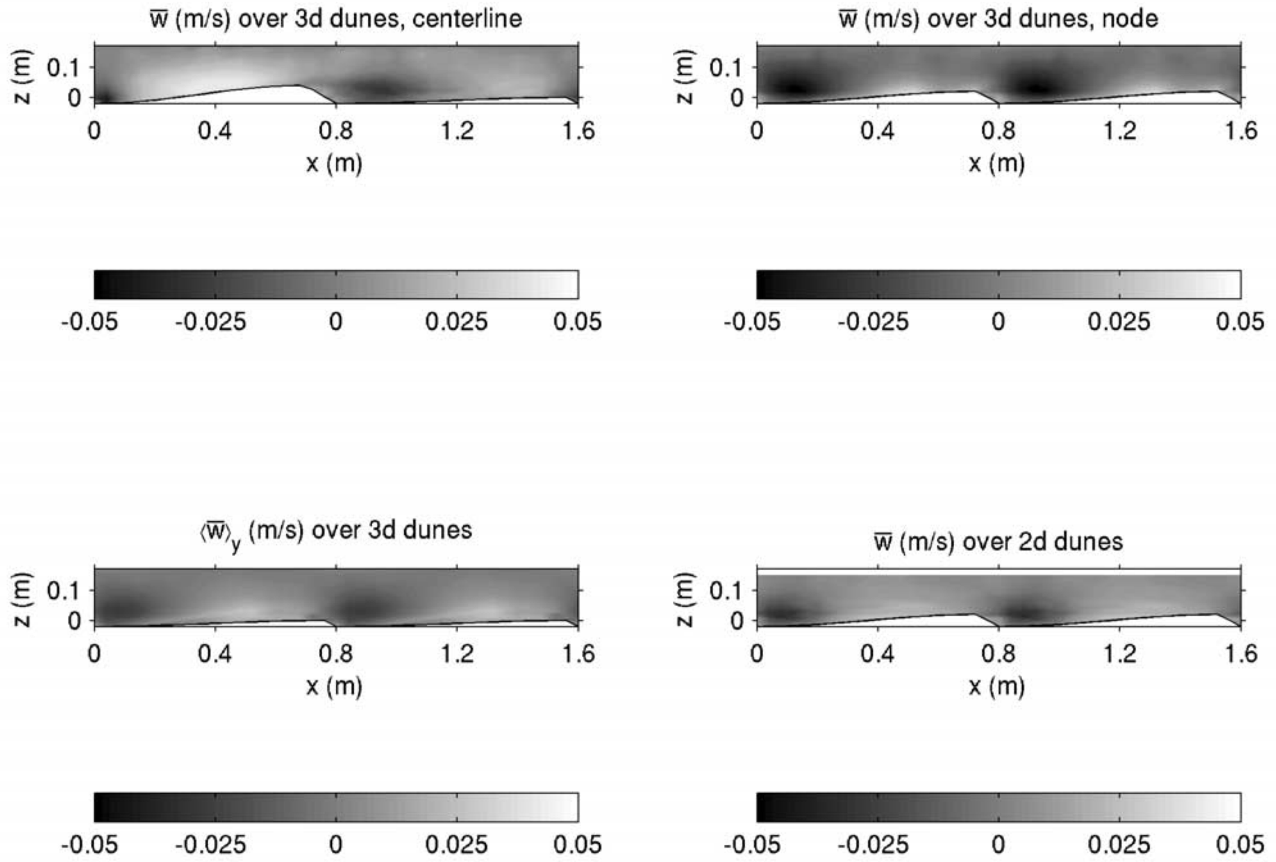

Figure 9. Mean vertical velocities for run T2 at (top left) the centerline and (top right) the node. Also shown are the cross-stream average of (bottom left) the vertical velocity for run T2 and (bottom right) the vertical velocity measured during run 2. See color version of this figure in the HTML.

measurements over 2-D dunes, with maximum stresses occurring in the separation zone at elevations just beneath the tops of the dune crests. However, quantitative differences were significant. The cross-stream average of the Reynolds shear stress measured during run T2 was only half of that measured during run 2. Local values of stresses were largest downstream of the nodal crests, while those in the trough region downstream of the highest crest were relatively diffuse. High stress values generated downstream of the highest crest penetrated to the interior of the flow over the lowest crest, while $-\overline{u'w'}$ was small throughout the interior of the node cross section.

[42] Figure 12 shows values of $-\overline{u'w'}$ measured during run T3. The results were consistent with the measurements during run T2, with stresses over the 3-D dunes only 50% of those measured over the 2-D dunes. Turbulent stresses were negligible in the upper 0.3 m of the water column at all cross-stream locations, and at the node of the crest line this region of low stress extended downward nearly to the top of the dune. These low turbulence levels were also present in measurements of the total turbulent kinetic energy, which are qualitatively similar to the shown measurements of $-\overline{u'w'}$ and can be seen in the electronic supplement. Turbulence production was also lower over the 3-D dunes, but like the 2-D dunes it was greatest just downstream of the dune crest at an elevation even with the crest (data not shown). Given that the friction coefficients of the 3-D dunes averaged 50% greater than those of the 2-D dunes, these lower levels of measured turbulence over the 3-D dunes present an apparent contradiction.

3.5. Streamwise-Averaged Flow Field

[43] The streamwise-averaged (equation (4)) mean velocities measured during run T2 are shown in Figure 13. Mean flow contours are shown along with dashed lines indicating the height of the crest lines of the two dune phases (Figure 2). Mean streamwise velocities were greatest on average over the node, as was shown previously. Additionally, these larger streamwise velocities were colocated with downward flow while the slower flows over the highest and lowest points of the crest line were colocated with upward flow, as shown in the lower left contour plot. The quiver plot shown at the lower right quadrant completes the picture, showing a system of four counterrotating secondary circulation vectors, with secondary current velocities of about 2 cm/s, which was just over 5% of the average flow rate for run T2. By directing faster streamwise flows toward the surface and slower streamwise flows toward the bed, the secondary currents appear to be generating a net downward momentum flux. It is possible that this flux could be

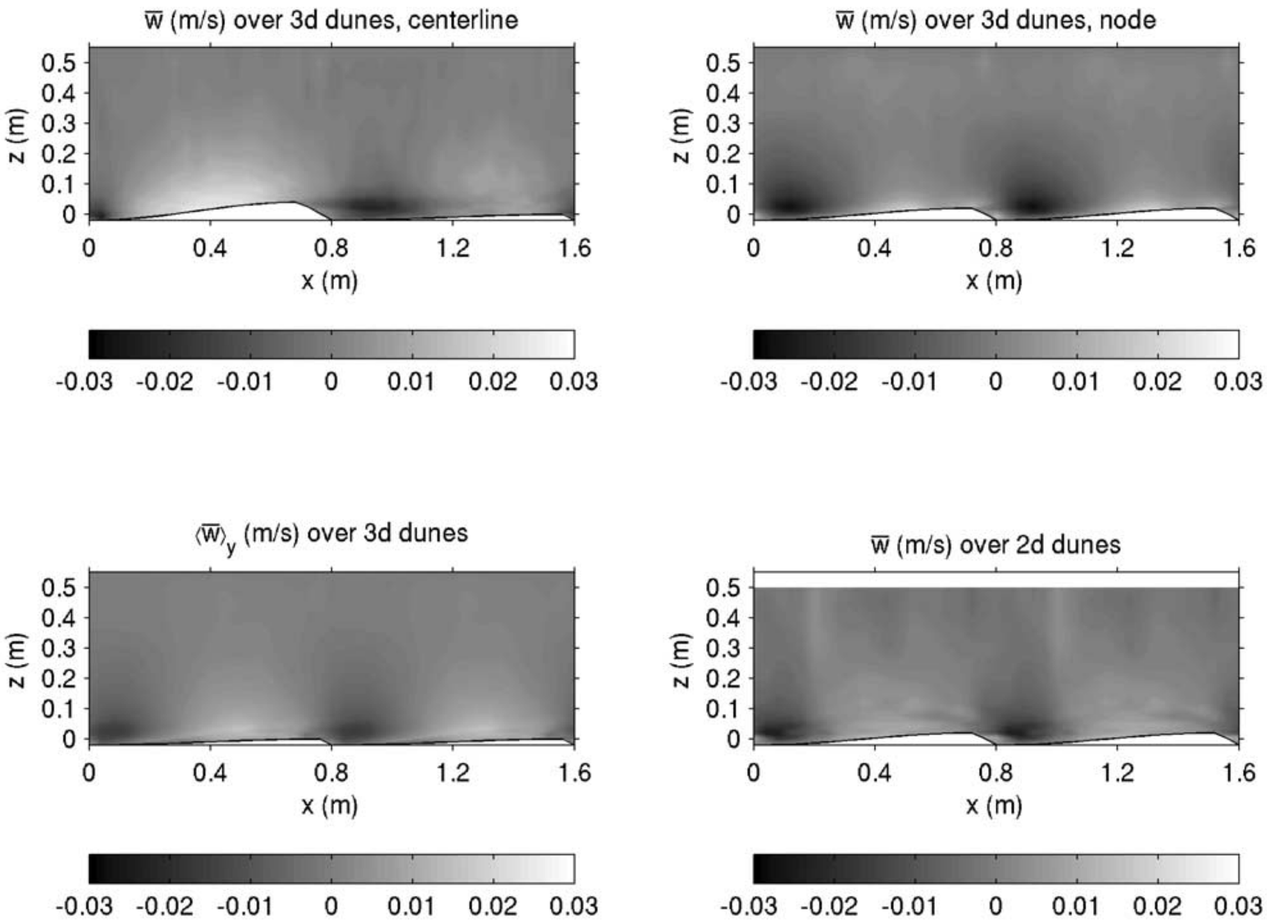

Figure 10. Mean vertical velocities for run T3 at (top left) the centerline and (top right) the node. Also shown are the cross-stream average of (bottom left) the vertical velocity for run T3 and (bottom right) the vertical velocity measured during run 3. See color version of this figure in the HTML.

carrying momentum that is not being carried by low levels of turbulence over the 3-D dunes.

[44] The streamwise-averaged mean velocities measured during run T3 were similar, as shown in Figure 14. Most of the secondary current was measured within the lower half of the water column, with maximum velocities of about 1 cm/s, or 4% of the mean flow rate. Cross-stream secondary currents were strongest at or below the dune crest line, while above they were more diffuse, owing to the greater depth of flow. However, in both cases the elevation of the center of the circulation cell, as defined by the point of reversal of cross-stream flow, was closer to the dune crest line than half the flow depth. Also present during run T3 were a second set of very weak secondary cells in the upper part of the water column, forming eight counterrotating cells.

[45] The streamwise averages of the Reynolds shear stresses and production of turbulence, $\wp$, measured during run T2 are shown in Figure 15. Turbulence production was obtained from the measurements using the following formula in Cartesian tensor notation with implicit summation [*Tennekes and Lumley*, 1989]:

$$\wp = -\overline{u_i' u_j'}\frac{1}{2}\left(\frac{\partial \bar{u}_i}{\partial x_j} + \frac{\partial \bar{u}_j}{\partial x_i}\right). \quad (5)$$

[46] Little to no vertical structure was present in $-\overline{u'v'}$, which changed only in the cross stream. The largest of the three components of Reynolds shear stress, $-\overline{u'w'}$, was relatively large below the dune crest line at all cross-stream locations, and greatest at the node of the crest line. Above the dune crest line, this was reversed, with relatively low stress values above the crest line node. The production of turbulence had a similar structure, as did the turbulent kinetic energy and velocity variances (data not shown; please see the electronic supplement animations or *Maddux* [2002]). Streamwise-averaged turbulent quantities during run T3 were similarly structured, as shown in Figure 16. The relative lack of vertical structure of $-\overline{u'v'}$ was again apparent. However, in this case it persisted through half the flow depth, which corresponded to the maximum depth at which there was noticable cross-stream shear in the streamwise velocity (Figure 14). Cross-stream asymmetries in $-\overline{u'w'}$ in the flow interior were much more pronounced during run T3, while the structure of production of turbulence was essentially no different than it was during run T2, being largest at or below the dune crest lines and negligible above.

[47] The cross-stream asymmetry of the turbulence field is a plausible source of the secondary currents. The cross-

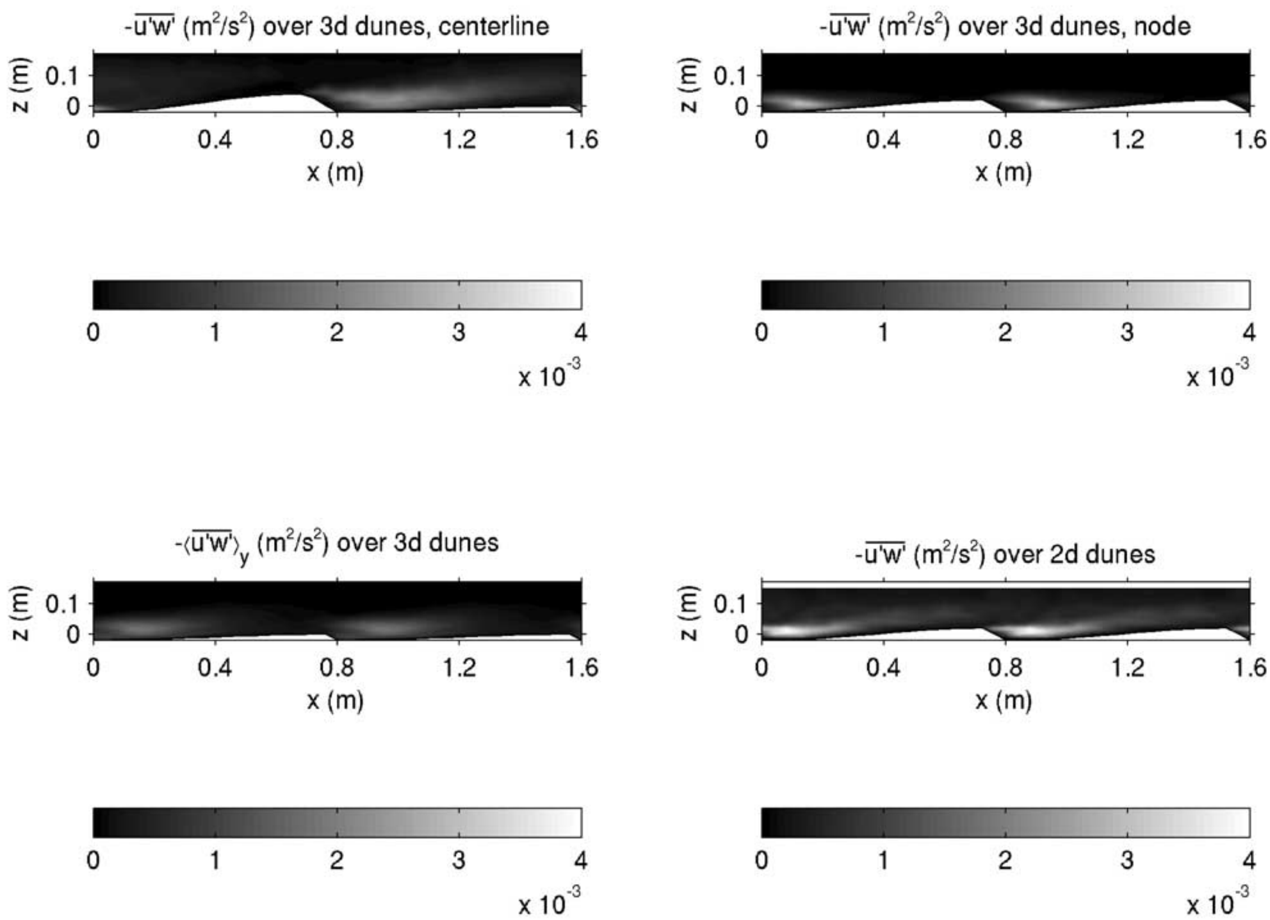

Figure 11. Reynolds shear stresses for run T2 at (top left) the centerline and (top right) the node. Also shown are the cross-stream average of (bottom left) the Reynolds shear stress for run T2 and (bottom right) the Reynolds shear stress measured during run 2. See color version of this figure in the HTML.

stream turbulence structure could potentially drive cross-stream flow from regions of high near-bed turbulence to regions of low near-bed turbulence. Furthermore, in the interior, cross-stream flow would be driven by the turbulence asymmetry in a similar fashion, but in the opposite direction to the near-bed flow. During both runs, interior regions of low $-\overline{u'w'}$ were collocated with downward flow and interior regions of high $-\overline{u'w'}$ were collocated with upward flow. All of these spatial structures observed in the streamwise-averaged turbulence field over 3-D dunes have been reported previously over smooth and rough longitudinal bed strips and over longitudinal sand ridges, with similar implications for the formation of secondary current cells [*Nezu and Nakagawa*, 1993].

3.6. Implications for Natural Dune Fields

[48] The study presented here is admittedly only a first step toward the study of dunes that more closely resemble the varied 3-D features found in nature. One possible next step could be to mold a series of natural 3-D dunes, as has been done with 2-D dunes and ripples [*Bennett and Best*, 1995, 1996] in the laboratory. Alternatively, field studies are becoming more detailed, with recent field observations having been made of the spatial variability in turbulence over dunes [*Williams et al.*, 2003]. It may soon be feasible to conduct detailed profiles of the turbulence structure of a 3-D flow field over natural dunes.

[49] Dunes in natural settings are often composed of individual dunes with discontinuous crest lines. This results in a 3-D dune field with high crest locations that are scattered in the horizontal. It is possible that this would permit more routing of flow around dune crests and hence more of the spatial variability of the turbulence and mean flow fields observed in this study. It could be argued that a random field of dunes would produce less reinforcement of nascent secondary current structures than were found in the mathematically precise dunes in our laboratory flume. On the other hand, these dunes were constructed as carefully as possible to be periodic and symmetric about the centerline, and yet *Maddux et al.* [2003] show that significant momentum fluxes were carried by asymmetries of the flow field. In a natural flow field with more variable bed shapes it is plausible that these asymmetries would be even larger.

4. Conclusions

[50] Detailed laboratory measurements of two different depths of turbulent open-channel water flow over fixed, artificial, asymmetric, sinuous-crested 3-D dune shapes were obtained in a tilting-recirculating flume. These were

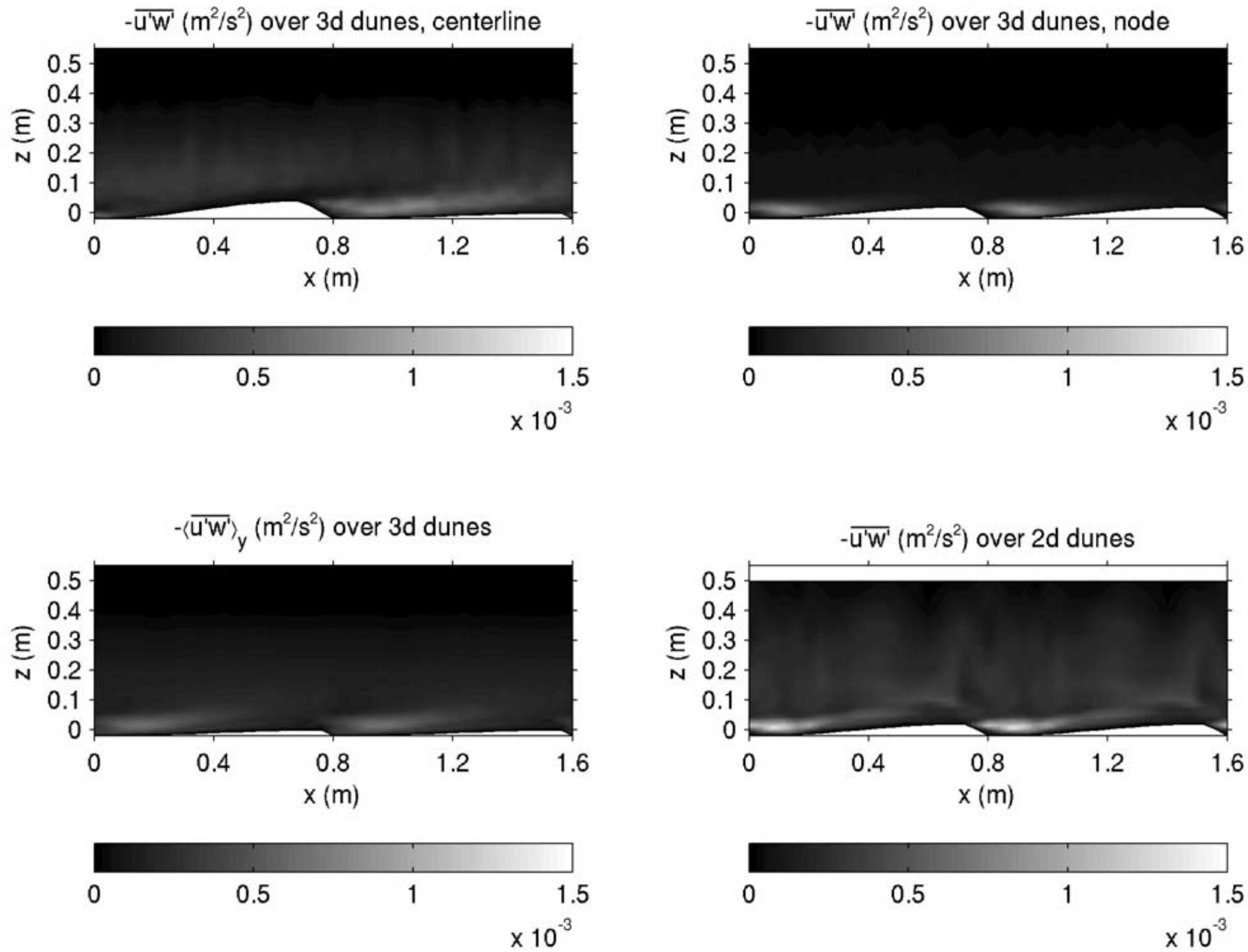

Figure 12. Reynolds shear stresses for run T3 at (top left) the centerline and (top right) the node. Also shown are the cross-stream average of (bottom left) the Reynolds shear stress for run T3 and (bottom right) the Reynolds shear stress measured during run 3. See color version of this figure in the HTML.

the first detailed measurements of turbulent open-channel flow over a three-dimensional dune bathymetry. Many of the general features frequently observed in flows over 2-D dunes were also observed over the 3-D dunes, including the separation of flow at the dune crest and generation of turbulence in the associated shear layer. The friction coefficients of the 3-D dunes were 50% higher on average in comparison to the friction coefficients of their 2-D counterparts when subjected to flows of similar depths and discharges. However, despite the larger friction of the 3-D dunes, the turbulence generated by them was much weaker than that generated by their 2-D counterparts, not only in the region of the shear layer and turbulent wake but also in the flow interior.

[51] The free surface response to 3-D dunes was two-dimensional and its cross-stream average precisely matched the response of the free surface to 2-D dunes. Mean streamwise velocities were largest over the node of the dune crest line rather than over the highest or lowest elevations of the crest line. The largest measured cross-stream free surface gradients and cross-stream velocities were in the trough, just downstream of the crest line nodes, with most of the cross-stream flow occurring close to the bed. A numerical shallow water model predicted a larger, more 3-D free surface response. The model underpredicted the cross-stream steering of the flow and overpredicted the acceleration of velocities over the highest part of the crest line, resulting in greatest streamwise velocities over the maxima of the dune crest line. The disparity between the vertically averaged model and the measurements suggest that nonhydrostatic effects are important; in other words, the steering of the flow occurs primarily in the near-bed region.

[52] The faster mean flow over the node of the dune crest line was collocated with relatively high levels of near-bed streamwise-averaged turbulence and lower levels of interior turbulence, while the slower flow over the highs and lows of the dune crests was collocated with low levels of near-bed turbulence and high levels of interior turbulence. These cross-stream gradients in the turbulence field could be responsible for the generation of observed secondary cells of streamwise-averaged vertical and horizontal motion. The secondary current cells directed the faster moving, less turbulent fluid downward and slower moving, more turbulent fluid upward.

[53] Since earlier observations of fluid flow over 2-D dunes have shown that the Reynolds stresses are the

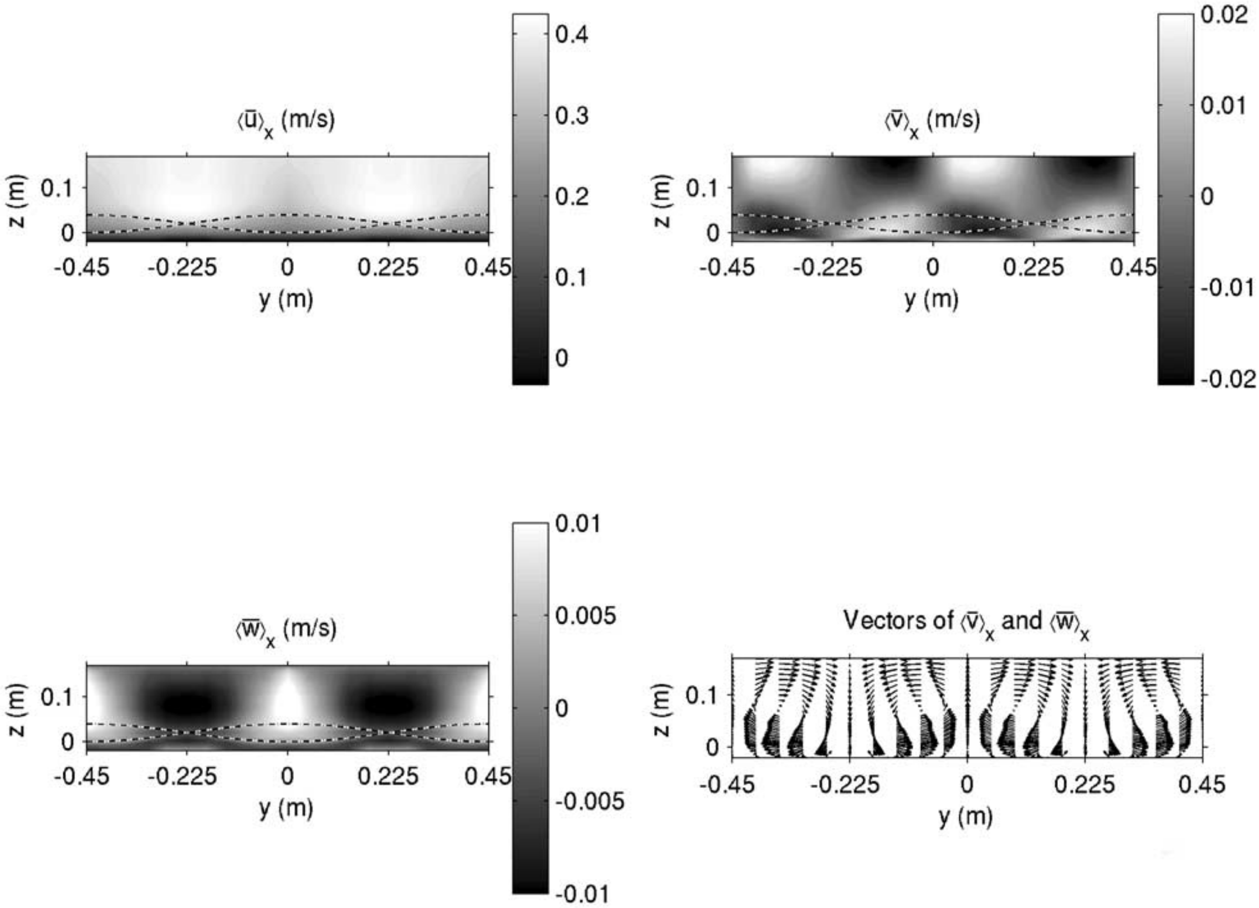

Figure 13. Streamwise-averaged mean velocities for run T2. Shaded contours denote the magnitude of each velocity component and quivers denote the vector field of streamwise-averaged cross-stream and vertical velocities. Dashed lines in the contour plots show the height and phase of the dune crest lines in this and subsequent *y-z* figures. See color version of this figure in the HTML.

principal carriers of momentum flux through the fluid, the higher friction coefficients of the 3-D dunes and lower Reynolds shear stresses present an apparent contradiction. The sinuous cross-shore structure of the mean streamwise flow in the interior coupled with the secondary circulation cells could be responsible for the remaining momentum flux. This hypothesis is tested by *Maddux et al.* [2003] using a spatial average applied to the equations of mass and streamwise momentum conservation. It will be shown that while the spatially averaged Reynolds shear stress cannot be used to predict the total boundary shear stress over the 3-D dunes. Furthermore, the complete formulation, which includes the effects of asymmetries in the mean flow and turbulence fields, results in improved agreement between estimates of total boundary shear stress based on spatially averaged momentum fluxes and other estimates, including the depth-slope product and the sum of form drag and skin friction.

Notation

C_f friction coefficient.

g acceleration due to gravity, m/s^2.

F arbitrary flow quantity.

$\overline{F}$ time-averaged flow quantity.

F' time-fluctuating component of a flow quantity.

$\langle F\rangle_x$ streamwise-averaged flow quantity.

$\langle F\rangle_y$ cross-stream-averaged flow quantity.

$\langle F\rangle_z$ depth-averaged flow quantity.

Fr Froude number.

h_0 mean flow depth, m.

H local dune height above trough, m.

$\langle H\rangle$ average (cross-stream) of dune height above trough, m.

L_f length occupied by fluid in streamwise-averaging domain, m.

$\wp$ production of turbulence, m^2/s^3.

R_h hydraulic radius, m.

S mean free surface (and bottom) slope(s).

u, v, w fluid velocities in x, y, z directions respectively, m/s.

U average fluid velocity in the flume measurement region, m/s.

u_* fluid shear velocity, m/s.

u_*^T shear velocity associated with total boundary shear stress, m/s.

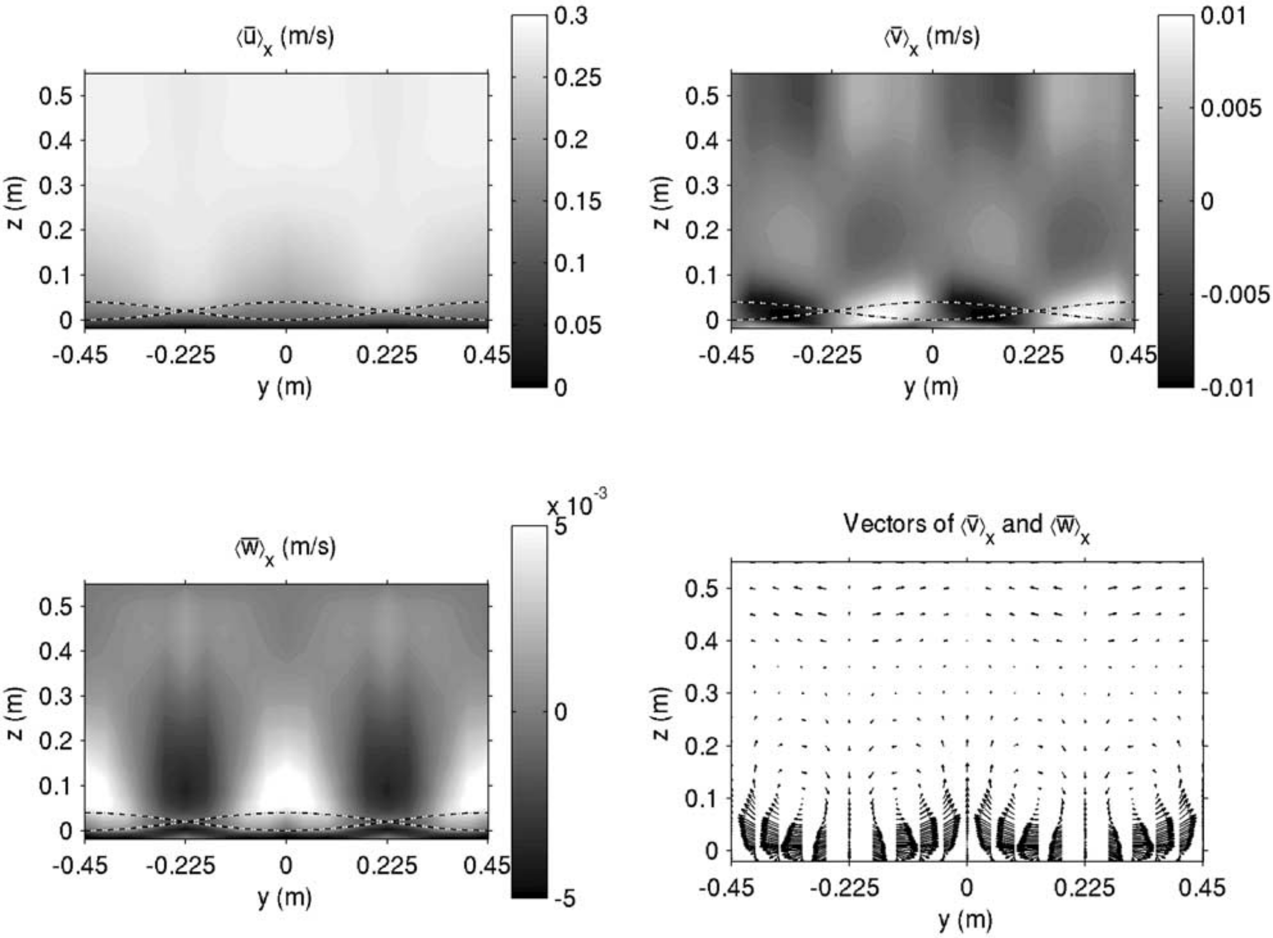

Figure 14. Streamwise-averaged mean velocities for run T3. Shown are shaded contours of mean velocity components and vectors of streamwise-averaged cross-stream and vertical velocity vectors. See color version of this figure in the HTML.

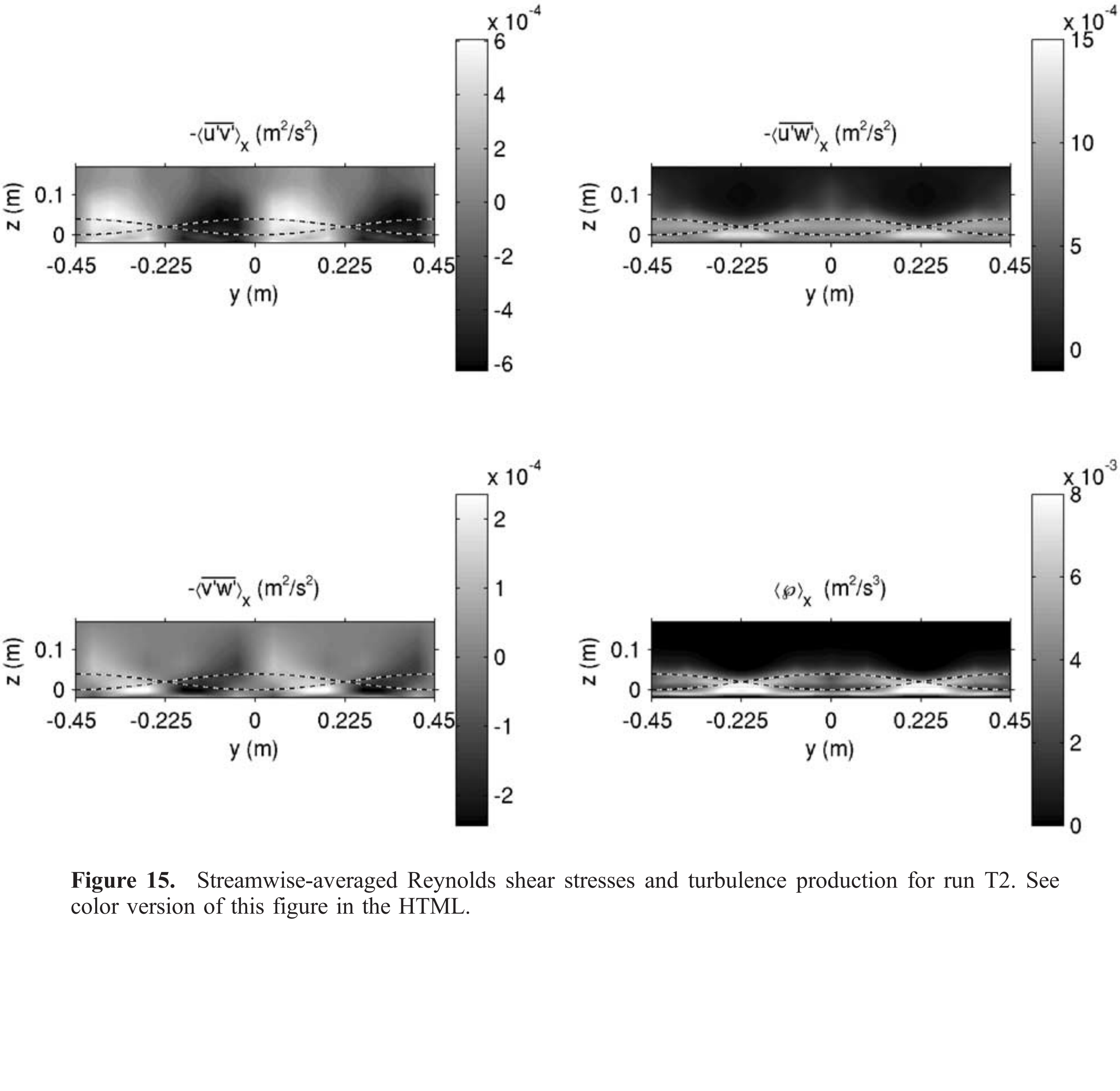

Figure 15. Streamwise-averaged Reynolds shear stresses and turbulence production for run T2. See color version of this figure in the HTML.

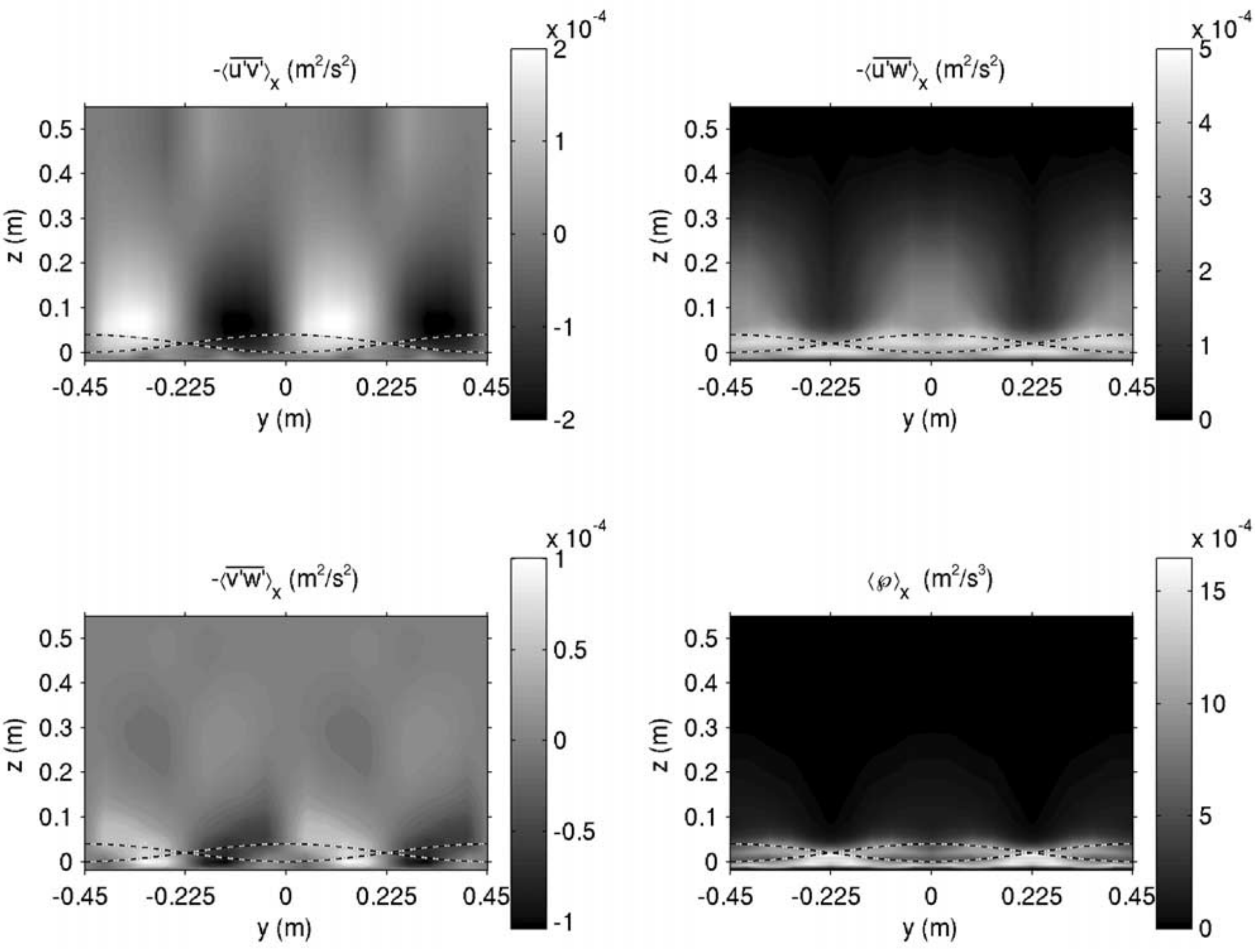

Figure 16. Streamwise-averaged Reynolds shear stresses and turbulence production for run T3. See color version of this figure in the HTML.

W_f width occupied by fluid in cross-stream-averaging domain, m.
x distance downstream, m.
x_1, x_2 upstream and downstream bounds of flume measurement region, m.
y distance cross stream, m.
y_1, y_2 cross-stream bounds of flume measurement region, m.
z distance above the mean bed elevation, m.
ζ local mean free surface elevation, m.
η local bed elevation, m.
λ local wavelength, distance from dune crest to dune crest, m.
$\langle\lambda\rangle$ average (cross stream) of dune wavelength, m.
ρ fluid density, kg/m^3.
τ fluid stress, N/m^2.
τ_T total stress, total boundary shear stress, N/m^2.

[88] **Acknowledgments.** This research was supported by the National Science Foundation through grants CTS-0120135, CTS-9634261, and CTS-9217804. We thank Manuela Lorenzi-Kayser, Verne Parmenter, Matthew Ressler, and Eric Schiller for assistance in experimental setup at the OEL. Finally, Jim Bennett, Mark Schmeeckle, two anonymous reviewers, the Associate Editor and the Editor provided thoughtful comments and suggestions that improved the quality of the manuscript.

References

Allen, J. R. L., *Sedimentary Structures, Their Character and Physical Basis*, 2 vols., Elsevier Sci., New York, 1982.

Ardhuin, F., T. G. Drake, and T. H. C. Herbers, Observations of wave-generated vortex ripples on the North Carolina continental shelf, *J. Geophys. Res.*, *107*(C10), 3143, doi:10.1029/2001JC000986, 2002.

Ashley, G. M., Classification of large-scale subaqueous bed forms: A new look at an old problem, *J. Sediment. Petrol.*, *60*(1), 160–172, 1990.

Bennett, S. J., and J. L. Best, Mean flow and turbulence structure over fixed, two-dimensional dunes—Implications for sediment transport and bed form stability, *Sedimentology*, *42*(3), 491–513, 1995.

Bennett, S. J., and J. L. Best, Mean flow and turbulence structure over fixed ripples and the ripple-dune transition, in *Coherent Flow Structures in Open Channels*, edited by P. J. Ashworth et al., pp. 281–303, John Wiley, Hoboken, N. J., 1996.

Best, J., and R. Kostaschuk, An experimental study of turbulent flow over a low-angle dune, *J. Geophys. Res.*, *107*(C9), 3135, doi:10.1029/2000JC000294, 2002.

Carling, P. A., E. Golz, H. G. Orr, and A. Radecki-Pawlik, The morphodynamics of fluvial sand dunes in the River Rhine, near Mainz, Germany. I. Sedimentology and morphology, *Sedimentology*, *47*(1), 227–252, 2000.

Cellino, M., and W. H. Graf, Experiments on suspension flow in open channels with bed forms, *J. Hydraul. Res.*, *38*(4), 289–298, 2000.

Costello, W. R., and J. B. Southard, Flume experiments on lower-flow-regime bed forms in coarse sand, *J. Sediment. Petrol.*, *51*, 849–864, 1981.

Dalrymple, R. W., R. J. Knight, and J. J. Lambiase, Bedforms and their hydraulic stability relationships in a tidal environment, Bay of Fundy, Canada, *Nature*, *275*, 100–104, 1978.

Elgar, S., B. Raubenheimer, and R. T. Guza, Current meter performance in the surf zone, *J. Atmos. Ocean Technol.*, *18*(10), 1735–1746, 2001.

Embabi, N. S., and M. M. Ashour, Barchan dunes in Qatar, *J. Arid Environ.*, *25*(1), 49–69, 1993.

Engel, P., Length of flow separation over dunes, *J. Hydraul. Div. Am. Soc. Civ. Eng.*, *107*(HY10), 1133–1143, 1981.

Flemming, B. W., Underwater sand dunes along the southeast African continental margin—Observations and implications, *Mar. Geol.*, *26*, 177–198, 1978.

Gabel, S. L., Geometry and kinematics of dunes during steady and unsteady flows in the Calamus River, Nebraska, USA, *Sedimentology*, *40*(2), 237–269, 1993.

Gallagher, E. L., S. Elgar, and E. B. Thornton, Megaripple migration in a natural surf zone, *Nature*, *394*(6689), 165–168, 1998.

Guy, H. P., D. B. Simons, and E. V. Richardson, Summary of alluvial channel data from flume experiments, 1956–1961, *U.S. Geol. Surv. Prof. Pap.*, *462-I*, 1–96, 1966.

Hanes, D. M., V. Alymov, and Y. S. Chang, Wave-formed sand ripples at Duck, North Carolina, *J. Geophys. Res.*, *106*(C10), 2575–2592, 2001.

Hinze, J. O., *Turbulence*, 790 pp., McGraw-Hill, New York, 1975.

Hsu, S.-T., and J. F. Kennedy, Turbulent flow in wavy pipes, *J. Fluid Mech.*, *47*(3), 481–502, 1971.

Hudson, J. D., L. Dykhno, and T. J. Hanratty, Turbulence production in flow over a wavy wall, *Exp. Fluids*, *20*(4), 257–265, 1996.

Julien, P. Y., and G. J. Klaassen, Sand-dune geometry of large rivers during floods, *J. Hydraul. Eng.*, *121*(9), 657–663, 1995.

Kostaschuk, R. A., A field study of turbulence and sediment dynamics over subaqueous dunes with flow separation, *Sedimentology*, *47*(3), 519–531, 2000.

Kostaschuk, R. A., and P. Villard, Flow and sediment transport over large subaqueous dunes—Fraser River, Canada, *Sedimentology*, *43*(5), 849–863, 1996.

Kraus, N. C., A. Lohrmann, and R. Cabrera, New acoustic meter for measuring 3d laboratory flows, *J. Hydraul. Eng.*, *120*(3), 406–411, 1994.

Lhermitte, R., and R. Serafin, Pulse-to-pulse coherent Doppler sonar signal processing techniques, *J. Atmos. Ocean Technol.*, *1*(4), 293–308, 1984.

Lohrmann, A., R. Cabrera, and N. C. Kraus, Acoustic-Doppler velocimeter (ADV) for laboratory use, in *Proceedings of Conference on Fundamentals and Advancements in Hydraulic Measurements and Experimentation*, pp. 351–365, Am. Soc. of Civ. Eng., Buffalo, N. Y., 1994.

Lohrmann, A., R. Cabrera, G. Gelfenbaum, and J. Haines, Direct measurements of Reynolds stress with an acoustic Doppler velocimeter, in *Proceedings of the IEEE Fifth Conference on Current Measurements*, pp. 205–210, IEEE Oceanic Eng. Soc., St. Petersburg, Fla., 1995.

Lyn, D. A., Turbulence measurements in open-channel flows over artificial bed forms, *J. Hydraul. Eng.*, *119*(3), 306–326, 1993.

Maddux, T. B., Turbulent open channel flow over fixed three-dimensional dune shapes, Ph.D. thesis, Univ. of Calif., Santa Barbara, 2002.

Maddux, T. B., S. R. McLean, and J. M. Nelson, Turbulent flow over three-dimensional dunes: 2, Fluid and bed stresses, *J. Geophys. Res.*, *108*, doi:10.1029/2003JF000018, in press, 2003.

McLean, S. R., and J. D. Smith, A model for flow over two-dimensional bed forms, *J. Hydraul. Eng.*, *112*(4), 300–317, 1986.

McLean, S. R., J. M. Nelson, and S. R. Wolfe, Turbulence structure over two-dimensional bed forms: Implications for sediment transport, *J. Geophys. Res.*, *99*(C6), 12,729–12,747, 1994.

McLean, S. R., J. M. Nelson, and R. L. Shreve, Flow-sediment interactions in separating flows over bedforms, in *Coherent Flow Structures in Open Channels*, edited by P. J. Ashworth et al., pp. 733, John Wiley, Hoboken, N. J., 1996.

McLean, S. R., S. R. Wolfe, and J. M. Nelson, Spatially averaged flow over a wavy boundary revisited, *J. Geophys. Res.*, *104*(C7), 15,743–15,753, 1999.

Nelson, J. M., and J. D. Smith, Mechanics of flow over ripples and dunes, *J. Geophys. Res.*, *94*(C6), 8146–8162, 1989.

Nelson, J. M., S. R. McLean, and S. R. Wolfe, Mean flow and turbulence fields over two-dimensional bed forms, *Water Resour. Res.*, *29*(12), 3935–3953, 1993.

Nelson, J. M., R. L. Shreve, S. R. McLean, and T. G. Drake, Role of near-bed turbulence structure in bed load transport and bed form mechanics, *Water Resour. Res.*, *31*(8), 2071–2086, 1995.

Nelson, J. M., J. P. Bennett, and S. M. Wiele, Modeling flow, sediment transport, and bed evolution in channels, in *Tools in Fluvial Geomorphology*, edited by M. Kondolph, and H. Piégay, pp. 539–576, John Wiley, Hoboken, N. J., 2003.

Nezu, I., and H. Nakagawa, *Turbulence in Open-Channel Flows*, 281 pp., A. A. Balkema, Brookfield, Vt., 1993.

Nikora, V. I., and D. G. Goring, ADV measurements of turbulence: Can we improve their interpretation?, *J. Hydraul. Eng.*, *124*(6), 630–634, 1998.

Raudkivi, A. J., Study of sediment ripple formation, *J. Hydraul. Div. Am. Soc. Civ. Eng.*, *89*(HY6), 15–33, 1963.

Raudkivi, A. J., Bed forms in alluvial channels, *J. Fluid Mech.*, *26*, 15–33, 1966.

Schlichting, H., *Boundary-Layer Theory*, 817 pp., McGraw-Hill, New York, 1979.

Shehata, W., T. Bader, O. Irtem, A. Ali, M. Abdallah, and S. Aftab, Rate and mode of barchan dunes advance in the central part of the Jafurah Sand Sea, *J. Arid Environ.*, *23*(1), 1–17, 1992.

Simons, D. B., and E. V. Richardson, Forms of bed roughness in alluvial channels, *Trans. Am. Soc. Civ. Eng.*, *128*, 284–302, Part 1, 1963.

Smith, J. D., and S. R. McLean, Spatially averaged flow over a wavy surface, *J. Geophys. Res.*, *82*(12), 1735–1746, 1977.

Snyder, W. H., and I. P. Castro, Acoustic Doppler velocimeter evaluation in stratified towing tank, *J. Hydraul. Eng.*, *125*(6), 595–603, 1999.

SonTek, Inc., ADV operation manual, version 1. 0, 30 pp., San Diego, Calif., 1995.

Sukhodolov, A., M. Thiele, and H. Bungartz, Turbulence structure in a river reach with sand bed, *Water Resour. Res.*, *34*(5), 1317–1334, 1998.

Tennekes, H., and J. L. Lumley, *A First Course in Turbulence*, 300 pp., Mass. Inst. of Technol., Cambridge, 1989.
Trowbridge, J., and S. Elgar, Turbulence measurements in the surf zone, *J. Phys. Oceanogr.*, *31*(8), 2403–2417, 2001.
van Mierlo, M. C. L. M., and J. C. C. de Ruiter, Turbulence measurements above artificial dunes, *Tech. Rep. TOW A55 Q789*, Delft Hydraul., Delft, Netherlands, 1988.
Venditti, J. G., and S. J. Bennett, Spectral analysis of turbulent flow and suspended sediment transport over fixed dunes, *J. Geophys. Res.*, *105*(C9), 2035–2047, 2000.
Villard, P., and R. A. Kostaschuk, The relation between shear velocity and suspended sediment concentration over dunes: Fraser Estuary, *Canada, Mar. Geol.*, *148*(1–2), 71–81, 1998.
Voulgaris, G., and J. H. Trowbridge, Evaluation of the acoustic Doppler velocimeter (ADV) for turbulence measurements, *J. Atmos. Ocean Technol.*, *15*(1), 272–289, 1998.
Wiberg, P. L., and J. M. Nelson, Unidirectional flow over asymmetric and symmetric ripples, *J. Geophys. Res.*, *97*(C8), 12,745–12,761, 1992.
Williams, J. J., P. S. Bell, and P. D. Thorne, Field measurements of flow fields and sediment transport above mobile bed forms, *J. Geophys. Res.*, *108*(C4), 3109, doi:10.1029/2002JC001336, 2003.
Yalin, M. S., Geometrical properties of sand waves, *J. Hydraul. Div. Am. Soc. Civ. Eng.*, *90*(HY5), 105–119, 1964.

T. B. Maddux, Department of Applied Ocean Physics and Engineering, Woods Hole Oceanographic Institution, Mail Stop 9, Woods Hole, MA 02543, USA. (tbmaddux@whoi.edu)

S. R. McLean, Department of Mechanical and Environmental Engineering, University of California, Santa Barbara, CA 93106, USA. (mclean@engineering.ucsb.edu)

J. M. Nelson, Water Resources Division, U.S. Geological Survey, Denver Federal Center, P.O. Box 25046, MS 413, Denver, CO 80225, USA. (jmn@usgs.gov)